Sensitivity of Mediterranean thermohaline circulation to gateway depth: A model investigation

Bahjat Alhammoud,[1,2] Paul T. Meijer,[1] and Henk A. Dijkstra[3]

Received 7 July 2009; revised 16 October 2009; accepted 29 December 2009; published 30 June 2010.

[1] The Neogene sedimentary record of the Mediterranean Sea holds evidence for changes in water properties and circulation. These paleoceanographic changes have been attributed to changes in the flow through the ocean gateway between the Mediterranean Sea and the Atlantic Ocean. We use an oceanic general circulation model to achieve quantitative, physics-based understanding of the effect of changes in the depth of the gateway such as may result from tectonic activity or variation in sea level. To isolate these effects we use idealized basin geometry and impose simplified atmospheric forcing. A reference experiment with present-day sill depth demonstrates that the model simulates reasonably well the main features of the present-day Mediterranean thermohaline circulation as inferred from observations and previous numerical studies. Subsequently, a series of sensitivity simulations is performed with different sill depths. The model results show that Mediterranean temperature, salinity, and thermohaline circulation depend strongly on sill depth. As the sill depth decreases, the upper overturning cell is quasi-linearly reduced in strength, while, contrary to what one would expect, the deep cell intensifies and does so in a nonlinear way. We find that a shoaling of the sill depth induces a "blocking effect" on the outflow waters, which creates a strong recirculation in the deep layers, strengthening the deep cell. Nevertheless, deep-water formation is reduced, and, as a consequence, the ventilation of the deep layers diminishes. We identify three different circulation modes of the Mediterranean thermohaline circulation depending on the sill depth: "shallow sill," "moderate sill," and "deep sill" modes coupled with strong, weak, and negligible blocking effects, respectively. Our results are consistent with the pre-Messinian paleoceanographic record of the Mediterranean Sea and may be useful to understanding the behavior of other land-locked basins, both extant and from the geological past.

Citation: Alhammoud, B., P. T. Meijer, and H. A. Dijkstra (2010), Sensitivity of Mediterranean thermohaline circulation to gateway depth: A model investigation, *Paleoceanography*, *25*, PA2220, doi:10.1029/2009PA001823.

1. Introduction

1.1. Objective and Approach

[2] The Mediterranean Sea, notwithstanding its land-locked nature, reaches typical open-oceanic depths and displays an active thermohaline circulation that resembles that of the much larger Atlantic Ocean. The basin-scale water properties and circulation are controlled by the combined action of atmospheric forcing and a narrow oceanic gateway: the Strait of Gibraltar. Atmospheric forcing consists of an evaporation that exceeds the sum of precipitation and rivers discharge. The ocean gateway limits the exchange of water with the open ocean and, together with the excess evaporation, gives rise to an antiestuarine circulation and causes the Mediterranean water to have a relatively high salinity.

[3] Because the mixing and the exchange through Gibraltar strait are considered as key processes in the Mediterranean thermohaline circulation (MTHC), several studies have been carried out to examine in detail the flow system in the strait [*Bethoux*, 1980; *Bryden and Stommel*, 1984; *Bryden et al.*, 1994; *Candela*, 2001; *Tsimplis and Bryden*, 2000; *Vargas et al.*, 2006]. The MTHC has been considered an important component of the climate system of the Eurafrican region because of the existence of mutual feedback mechanisms [*Li et al.*, 2006; *Lionello et al.*, 2006; *Xoplaki et al.*, 2004]. In addition, the MOW transports a huge amount of salt into the North Atlantic, where it may affect the strength of the Atlantic thermohaline circulation [*Rogerson et al.*, 2006; *Thorpe and Bigg*, 2000]. The MTHC and the gateway exchange form a thermodynamically coupled system where the Atlantic Ocean is a heat source and salt sink for the Mediterranean Sea [*Somot et al.*, 2006]. Hence, any change in the transport through the strait (e.g., climatic variability, tectonic processes, etc.) would induce some perturbations into this system's equilibrium.

[4] Straddling the boundary between two converging lithospheric plates, the Mediterranean Sea has been subject to profound changes in geometry during the last tens of millions of years. Progressive collision between Africa/Arabia and Eurasia led to the disruption of the connection to the Indian

[1]UCG, Department of Earth Sciences, Faculty of Geosciences, Utrecht University, Utrecht, Netherlands.
[2]Now at Laboratoire de Météorologie Dynamique, Ecole Polytechnique, Palaiseau, France.
[3]UCG, IMAU, Department of Physics and Astronomy, Utrecht University, Utrecht, Netherlands.

0883-8305/10/2009PA001823

Ocean in middle Miocene time [*Meulenkamp and Sissingh*, 2003; *Popov et al.*, 2004; *Rögl*, 1998]. The region of the connection to the Atlantic Ocean has likewise been the site of strong tectonic activity [*Jolivet et al.*, 2006; *Meulenkamp and Sissingh*, 2003]. Prior to the early Messinian the Mediterranean was connected to the Atlantic via two gateways or marine corridors: the Betic corridor across the southern Iberian peninsula and the Rif corridor through northwestern Africa.

[5] Albeit in incomplete fashion, the history of water properties and circulation is reflected in the fossil content and lithological and chemical aspects of the sediments that accumulated on the seafloor. The Neogene record from the Mediterranean basin, exposed due to later tectonic uplift or sampled in ocean drilling, is characterized, for example, by the regular occurrence of organic-rich layers (sapropels). These are first and foremost considered to express the control on circulation of orbitally induced climate change [*Rohling and Hilgen*, 1991; *Rossignol-Strick*, 1985] but the very fact that organic-rich sediments could form is thought to be due to the land-locked nature of the basin. Perhaps the clearest expression of the control exerted by the ocean gateway is formed by the thick interval of evaporites of Messinian age [*Duggen et al.*, 2003; *Krijgsman et al.*, 1999a; *Rohling et al.*, 2008]. While the deposition of these gypsum and halite layers is likely related to a closed or nearly closed connection to the outside ocean [*Hsü*, 1983; *Kouwenhoven and van der Zwaan*, 2006], the preevaporitic proxy record also holds evidence for weaker reductions in connectivity. By early Messinian time the Betic strait was most likely closed and subsequent paleoceanographic changes inferred from the Mediterranean record have been ascribed to changes in the depth of the Rif corridor [*Hsü*, 1983; *Kouwenhoven and van der Zwaan*, 2006]. This notion, that basin properties and circulation depend on sill depth, is also to be found in the work of *Sierro et al.* [2003] regarding the Betic corridor and that of *Köhler et al.* [2010] with reference to the predecessor of the Strait of Sicily. Thus, without wanting to ignore the role of atmospheric forcing (i.e., climate), it appears that the ocean gateway exerts an important control on circulation.

[6] To our knowledge, except for the work of *Meijer et al.* [2004], little quantitative work has been done on the interaction between tectonic processes and Mediterranean thermohaline circulation for times prior to the Messinian. Several studies showed the importance of gateways on ocean circulation on the global scale, but (except for the work of *Murdock et al.* [1997], who considered both an open and a closed gateway through the Panama isthmus) none of these studies focused on the importance of sill depth [*Haug and Tiedemann*, 1998; *Mikolajewicz et al.*, 1993; *von der Heydt and Dijkstra*, 2006].

[7] The purpose of this paper, then, is to try and achieve quantitative, physics-based understanding of the influence exerted by the oceanic gateway on Mediterranean water properties and thermohaline circulation. While we realize that climate variation will have had its effect on circulation also, we here focus on the effect of variation in the depth of the gateway sill such as may result from tectonic activity or variation in sea level. Model studies similar to ours but focusing on the role of temporal changes in atmospheric forcing are, for example, by *Bigg* [1994], *Myers et al.* [1998a, 1998b], *Myers and Haines* [2002] and *Meijer and Dijkstra* [2009]. Our tool is an ocean general circulation model, the Princeton Ocean Model (POM), used in a coarse horizontal resolution (1° × 1°). In order to be able to focus on the role of the gateway, we reduce the problem to its essence: a land-locked basin connected to an "ocean" by a single gateway (Figure 1). The model is not meant to represent as realistically as possible the present-day Strait of Gibraltar but rather to capture the effects of a general "bottle neck" between ocean and basin on the water properties and circulation of the basin. The much idealized geometry (explained in more detail below) is combined with a likewise idealized atmospheric forcing consisting of a uniform and constant net evaporation and a relaxation of sea surface temperature to a constant atmospheric temperature that varies with latitude only. The "minimal model" thus obtained proves capable of capturing qualitatively the main features of the basin-scale thermohaline circulation of the present-day Mediterranean Sea. The model is used to systematically explore the effects of gateway depth: starting from the same initial temperature and salinity and applying the same atmospheric forcing, we calculate the steady state circulation for different sill depths. In our interpretation and application of the model results we will consider the different simulations as representing different points in time. However, it is important to point out that we do not calculate the response to a sill depth that actually changes with time. The time scale over which sill depth will have varied due to tectonic causes (1 Myr) or due to sea level change (10 kyr to 1 Myr) is much longer than the time needed by the basin to adjust to the new configuration (100 yr). The geological record may thus be considered to reflect a sequence of steady state situations. Model results will be compared to observations, and to interpretation based on these observations, of the preevaporitic sediment record and should provide a good basis for understanding other aspects of the Mediterranean paleoceanography. Moreover, due to its idealized setup, our results have a generic quality and should be applicable to other land-locked basins as well.

1.2. Present-Day Mediterranean Thermohaline Circulation

[8] Since the 1970s, the Mediterranean thermohaline circulation (MTHC) has been well documented [*Haines and Wu*, 1995; *Millot*, 1987; *Ovchinnikov*, 1966; *Roether et al.*, 1996; *MEDOC Group*, 1970; *Robinson et al.*, 1992; *Wüst*, 1961] and consists of external and internal cells. The external cell is characterized by a zonal overturning circulation in the upper 500 m connecting the Mediterranean Sea to the Atlantic Ocean. At the surface, relatively fresh Atlantic water (AW) flows eastward in the upper 100–200 m of the basin, becoming warmer and saltier because of the air-sea interaction and mixing with the saltier surface Mediterranean water. In the easternmost part of the basin (the Levantine basin), a relatively dense and high-salinity water mass is formed due to winter cooling of the AW. This water mass circulates westward through the basin in the intermediate depths between 200 and 800 m and is called Levantine Intermediate Water. This water mass plays a crucial role in the preconditioning of the deep-water formation. The internal cells are driven by the

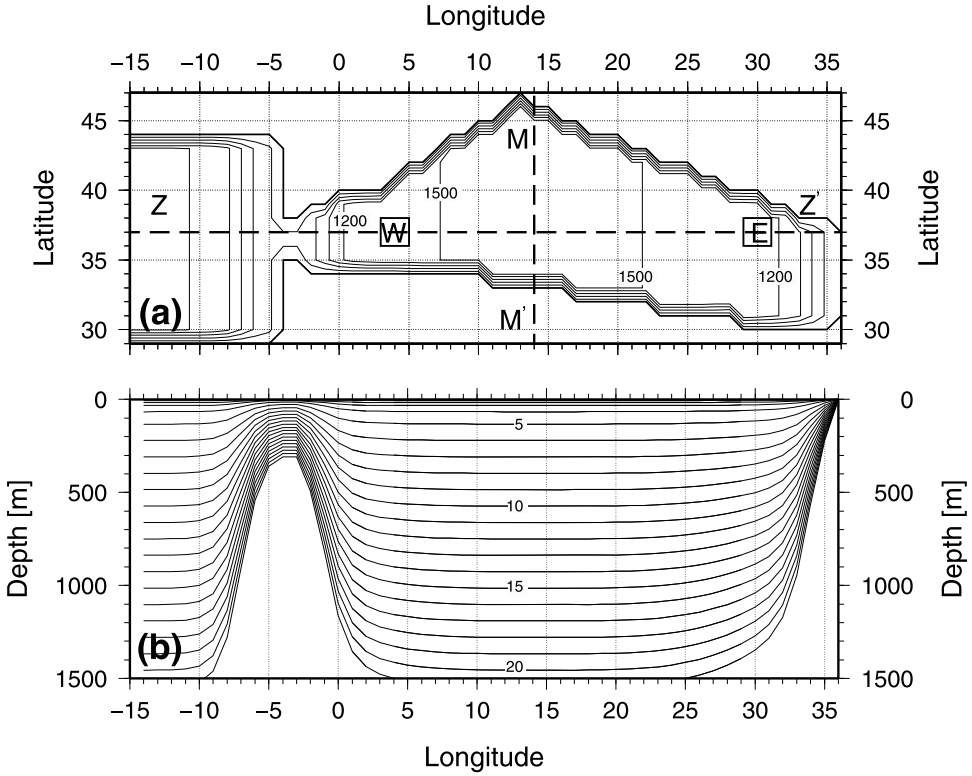

Figure 1. (a) Model grid and corresponding topography (contour interval 300 m). Dashed lines ZZ′ and MM′ indicate the position of zonal and meridional cross sections through the basin, respectively. Boxes W and E are the averaging window for time series in Figure 8. (b) Vertical section at ZZ′ of sigma levels showing the sill shape, western and eastern boundaries.

deep-water formation in the northern part of the western and eastern basins. The process of the deep water formation in the Mediterranean Sea is well described by *Marshall and Schott* [1999]. A dense water mass is formed via convection events driven by intense local cooling from winter storms in the high-latitude parts of the basin (Gulf of Lions, Adriatic Sea and recently the Aegean Sea and Levantine basin). This dense water mass sinks to the bottom layers and spreads southward then westward before joining the Mediterranean outflow water (MOW) through Gibraltar strait [*Pinardi and Masetti*, 2000].

[9] The paper is organized as follows: section 2 introduces the model setup used for this study. Section 3 presents the model results. In section 4, the model results are analyzed and discussed. Finally, summary and conclusions are presented in section 5.

2. Model Setup

[10] We use the Princeton Ocean Model (POM) which is a three-dimensional, free surface, hydrostatic, bottom-following vertical sigma coordinate, primitive equation model [*Blumberg and Mellor*, 1987]. Several studies have successfully applied the POM to the Mediterranean Sea [*Drakopoulos and Lascaratos*, 1999; *Horton et al.*, 1997; *Korres et al.*, 2002; *Lascaratos and Nittis*, 1998; *Zavatarielli and Mellor*, 1995] and to Gibraltar strait [*Sannino et al.*, 2002]. In order to achieve computational efficiency, a mode splitting technique is employed for the external 2-D (barotropic) and the internal 3-D (baroclinic) modes. The model numerically solves the momentum equations, continuity equation and tracer (temperature and salinity) equations in a finite difference form along with a nonlinear equation of state $\rho = \rho(\theta, S, P)$ coupling the two active tracer fields to the velocity field [*Mellor*, 1991].

[11] The horizontal mixing coefficients A_M (viscosity) and A_H (diffusivity) are calculated using a Smagorinsky formulation [*Mellor and Blumberg*, 1985], and can be formulated as, $(A_M, A_H) = (C_{vis}, C_{dif})\,\Delta x \Delta y[(\frac{\partial u}{\partial x})^2 + \frac{1}{2}(\frac{\partial v}{\partial x} + \frac{\partial u}{\partial y})^2 + (\frac{\partial v}{\partial y})^2]^{\frac{1}{2}}$ where u and v are the zonal and meridional velocity components respectively and C_{vis}, C_{dif} are constants. Based on many sensitivity experiments, we set the value of turbulent Prandtl number, $Pr = C_{vis}/C_{dif} = 250$. The vertical mixing coefficients K_M and K_H are calculated using the *Mellor and Yamada* [1982] turbulence closure scheme which yields small values of vertical viscosity and diffusivity near the stable thermocline depths. An exponential form is applied for the vertical viscosity in the deep layers (>500 m).

[12] A model study with a fine grid resolution is highly resource intensive and too expensive to use for simulations more than a few decades. Instead, we choose for a relatively coarse resolution of the horizontal grid ($\Delta x = 88$ km and $\Delta y = 111$ km). The vertical grid has 21 sigma levels, where $\sigma = (z - \eta)/(H - \eta)$, $\eta(x, y)$ and $H(x, y)$ are the surface elevation and water depth, respectively. The sigma layers are concen-

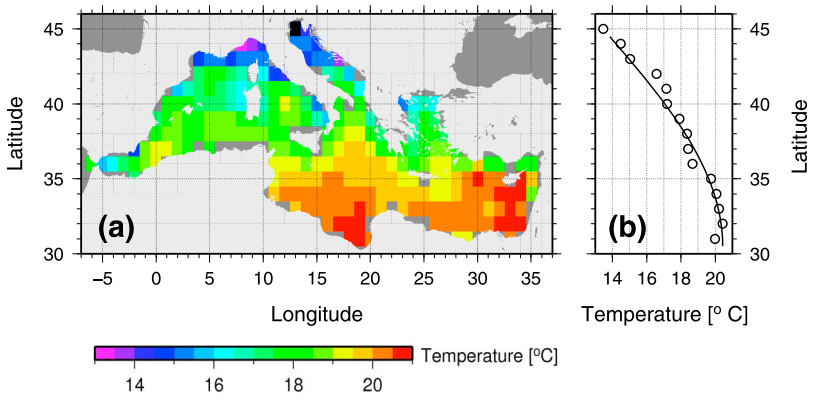

Figure 2. (a) Annual mean air temperature over the Mediterranean Sea (data are from the ECMWF as processed by G. Korres, Athens; http://pelagos.oc.phys.uoa.gr/mfstep). (b) Circle, zonal average of Figure 2a; solid line, smooth approximation of zonal averages.

trated in the upper water column to resolve the thermocline (Figure 1b). The time steps for the external and the internal modes are 240 s and 7200 s respectively.

[13] As we are interested in basin-scale features of the MTHC, we represent the Mediterranean Sea as a single idealized basin (Figure 1). The outline of the idealized basin is chosen to roughly follow the outer contours of the present Mediterranean Sea. The model basin thus approximately occupies the same longitudinal and, more relevantly so, latitudinal, range as the actual Sea. The basin extends from 29°N to 46°N in latitude and from 15°W to 37°E in longitude and includes a small part of the Atlantic Ocean. By deliberately not representing the Italian peninsula and the island of Sicily, a single basin is obtained with a single "upper corner" situated at relatively high latitude. With this corner geometry, we anticipate to mimic processes that currently occur in the Gulf of Lions and Adriatic Sea/northern Ionian Sea. Our aim is to capture once, the processes and circulation features that are, in the present-day Mediterranean Sea, found twice: in the western as well as in the eastern subbasin. Apart from near the sill and the eastern coastline the model depth is set at 1500 m, roughly the average depth of the present Mediterranean. In order to resolve the flow within the oceanic gateway a minimum of two grid points in the north-south direction is needed. With the 1° resolution of the model this results in a gateway width of 222 km. While noting that the Mediterranean-Atlantic gateway may well have been wider in the past [*Benson et al.*, 1991], our model gateway is certainly wide compared to the present-day Strait of Gibraltar (13–22 km). As we will demonstrate below, notwithstanding the coarsely resolved gateway, our model yields strait transport that are of the same order of magnitude as that observed for present-day Gibraltar strait. Most importantly, however, the model captures well the effect of the gateway on basin circulation. The east-west bathymetric profile of the sill as well as of the eastern boundary of the basin is defined by a hyperbolic tangent functional form (Figure 1b). The maximum bottom slope between two adjacent grid cells is set to $\Delta H/H < 0.75$ to satisfy the hydrostatic consistency conditions and hence the model solution stability [*Mellor et al.*, 1994].

[14] Initial conditions consist of a uniform temperature (T) and salinity (S) of 20°C and 35 psu, respectively. These values of T and S are chosen to keep the characteristics of the inflow waters through Gibraltar strait close to the AW characteristics. It is worth to note that the model shows the same behavior for different initial conditions. A constant and idealized atmospheric forcing of heat and freshwater fluxes is applied. This forcing is chosen to be close to the present-day climatology value. The net evaporation is taken constant at 1 m/yr, a value that is near the middle of the range of estimates for the present-day Mediterranean (0.5 to 1.3 m/yr; as compiled by *Meijer and Krijgsman* [2005]). The sea surface temperature (SST) over the Mediterranean basin is relaxed to a best fit of zonal average of annual mean field from present observation (Figure 2). The restoring time scale is τ_T = 15 days. Many sensitivity experiments showed that the wind stress does not change the thermohaline circulation pattern, but only intensifies the upper overturning cell [*Myers et al.*, 1998b; *Winton and Sarachik*, 1993]. Hence, consistent with our search for a minimal model, the forcing was restricted to SST relaxation and freshwater flux (evaporation minus precipitation, E−P) only.

[15] The model domain has an open boundary on its western side. For the barotropic mode, we impose a free radiation condition for the normal to the open boundary depth-averaged velocity and a zero-gradient condition for the free surface elevation. For the baroclinic mode, we apply a Sommerfeld radiation condition for the normal to the open boundary internal velocity whereas for the meridional velocities are put to zero. We impose a depth-averaged zonal velocity at the western boundary to keep the water volume conserved. In other words, the total inflow through the open boundary compensates the freshwater loss through the basin surface. This type of boundary conditions has been successfully applied in previous simulations of POM [*Beckers et al.*, 2002; *Ezer and Mellor*, 1994]. In the case of inflow through the boundary, temperature and salinity are imposed to prescribed values (equal to the initial conditions). In addition, we impose a buffer zone between 15°W and 7°W where salinity and temperature are damped to the initial values.

The damping coefficient varies from 3 months at 7°W to one month at 15°W and decreases exponentially in the deep layers (>500 m).

3. Model Results

[16] A reference experiment is performed combining the idealized Mediterranean basin with the idealized present-day atmospheric forcing and present-day sill depth of 300 m (hereinafter SD300:REF). In order to isolate the effect of the sill depth, many experiments are performed with sill depths between 50 m and 900 m. Apart from the depth of the sill these simulations are equivalent to the reference experiment. We will refer to the simulations as SD50 to SD900. The model starts from rest and is integrated for 1000 years for each sill depth. The run time is 3.4 h per 100 model years on a x86_64 Linux OS cluster with 2 GHz dual processor (dual core AMD Opteron) and 4 GB internal memory per node.

3.1. Reference Experiment

3.1.1. Overall Properties and Hydrology

[17] As explained, we will first present results for the reference experiment in which the sill is located at its present-day depth of 300 m. These results will be validated using observations and other modeling studies. In Figure 3, we present the temporal evolution of the model variables from the reference experiment and both sensitivity experiments (SD300:REF, SD100 and SD500 respectively). Figure 3a shows the spin-up of the circulation as expressed by the mean kinetic energy measure. This measure is defined as the basin average of flow speed squared where "basin" is taken to refer to the model domain east of the sill, i.e., from 5°W to 36° E. The basin mean kinetic energy approaches a stationary value on a timescale of around 200 years. The temperature and salinity reach an equilibrium state (~17.8°C, ~37.5 psu) in about 300 years (Figure 3b). The volume transport through the gateway reaches the equilibrium state (~1.92 Sv; 1 Sv = 10^6 m^3s^{-1}) after around 250 years (Figure 3a). The net flow (inflow minus outflow) for the equilibrium state is 91.7×10^{-3} Sv which is the same as the net freshwater loss through the basin surface.

[18] In order to illustrate the water mass distribution in the basin, we plot west-east and north-south vertical sections through the basin for the salinity (Figure 4) and temperature (Figure 5) averaged over the last 10 years of the run. We choose the presentation of these sections from the shallow sill to the deepest one (SD100, SD300 and SD500) to facilitate the comparison later on in the results and discussion sections. The vertical sections through the reference experiment (Figures 4c, 4d, 5c, and 5d) display a fresh and warm (<37.2 psu, > 18.7°C) surface water mass which occupies the surface layer shallower than 300 m. The intermediate depth between 300 and 800 m is occupied by a large tongue with a salinity maximum > 37.6 psu and a temperature ranging from 17.9 to 18.3°C. We refer to this water mass as intermediate water. The minimum temperature (<17.5°C) associated with low salinity values of < 37.6 psu is found in the deep layers of the basin (>1000 m) corresponding to the Mediterranean deep water. One may note that the temperature in the Atlantic box deeper than 300m is warmer than the Mediterranean outflow waters. Despite these unrealistic temperature values, the density difference between the Atlantic box and the Mediterranean outflow waters is sustained close to the observed value due to the dominant effect of the salinity. Another experiment has been performed with temperature 5°C colder than the initial conditions of the reference experiment. The resulting equilibrium state shows that the temperature of the water column is colder by ~5°C while the model behavior remains unchanged.

[19] Figure 4c demonstrates clearly the maximum salinity isohalines outcropping the surface in the easternmost part of the basin (equivalent in position to the Levantine basin). The upward sloping from east to west of the isohalines and isotherms and their steep orientation in the eastern part of the basin express the relatively dense intermediate water sinking to about 500 m depth and tending to spread westward. In the north-south section (Figures 4d and 5d) we observe deep convection (dense-water sinking) in the northern part of the basin as expressed by the homogenized water column.

3.1.2. General Circulation

[20] Figures 4c and 5c show the establishment of sharp salinity and temperature fronts along the strait separating the fresh, warm and light water from the saline, cold and dense water over the sill. The antiestuarine circulation is well reproduced with the freshwater inflow at the surface and the dense-water outflow in the deep layers through the gateway. A profile of east-west oriented velocity as a function of depth, monitored right over the sill in the center of the gateway (Figure 6b), clearly shows the inflow overlying the outflow. The velocity changes sign somewhat below the middle of the water column. The interface between surface and deep water deepens from the east to the west. The outflow water cascades over the sill to the bottom layers in the Atlantic box. The horizontal distribution of the salinity on the bottom sigma level (not shown) shows a northward stream of the Mediterranean outflow in the Atlantic Ocean. In a north-south salinity section across the strait (Figure 6b) we observe isohalines tilted toward the south: the relatively fresh inflow from the Atlantic appears to hug the southern side of the gateway and the denser outflow is concentrated on the northern side. This configuration is as expected due to Coriolis force acting in a relatively wide strait [*Gill*, 1982; *Hermann et al.*, 1989].

[21] An overturning stream function analysis provides the best information on the overall dynamics of the basin because it allows us to quantify all changes in depth and transport of the water masses. Indeed, it nicely captures the circulation at the scale of interest to us, that of the whole basin. Figure 7 presents the zonal and meridional stream function of the basin. The overall structure of the zonal stream function for the reference experiment is characterized by two distinct cells (Figure 7c). The external or upper zonal cell, which connects the Mediterranean Sea to the Atlantic Ocean, is located in the upper 1000 m. In this cell the water circulates in a clockwise sense (i.e., with the eastern end of the basin shown to the right) showing a downwelling in the eastern part of the basin and an upwelling right to the east of the gateway. Below this upper cell, there is the internal or deep (counterclockwise) cell which occupies the deep layers in the eastern part of the basin and showing an upwelling near the eastern boundary. The zonal overturning stream function shows a maximum value

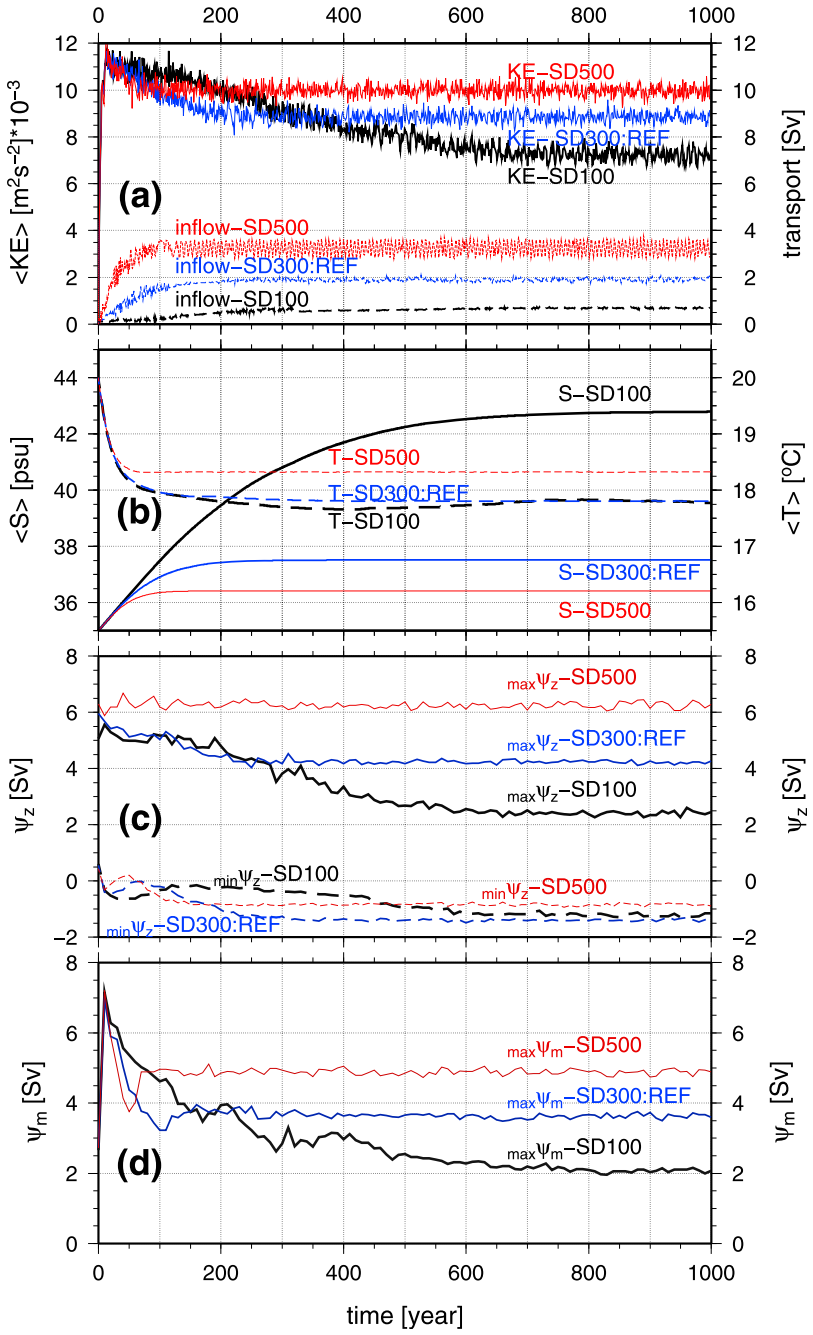

Figure 3. Time series of key model variables for the different simulations SD300:REF (blue), SD100 (black), and SD500 (red). (a) Solid line, kinetic energy measure (left vertical axis); dashed line, volume transport through the gateway (in Sv; 1 Sv = 10^6 m^3s^{-1}, right vertical axis). (b) Solid line, basin-averaged salinity $\langle S \rangle$; dashed line, basin-averaged temperature $\langle T \rangle$. (c) Decadally smoothed extrema of Mediterranean zonal overturning (in Sv). Solid line, maximum value in the upper 1000 m; dashed line, minimum value in the lower 500 m. (d) Decadally smoothed maximum value of the Mediterranean meridional overturning (in Sv) in the central northern basin (between 3°W and 36°E and north of 38°N).

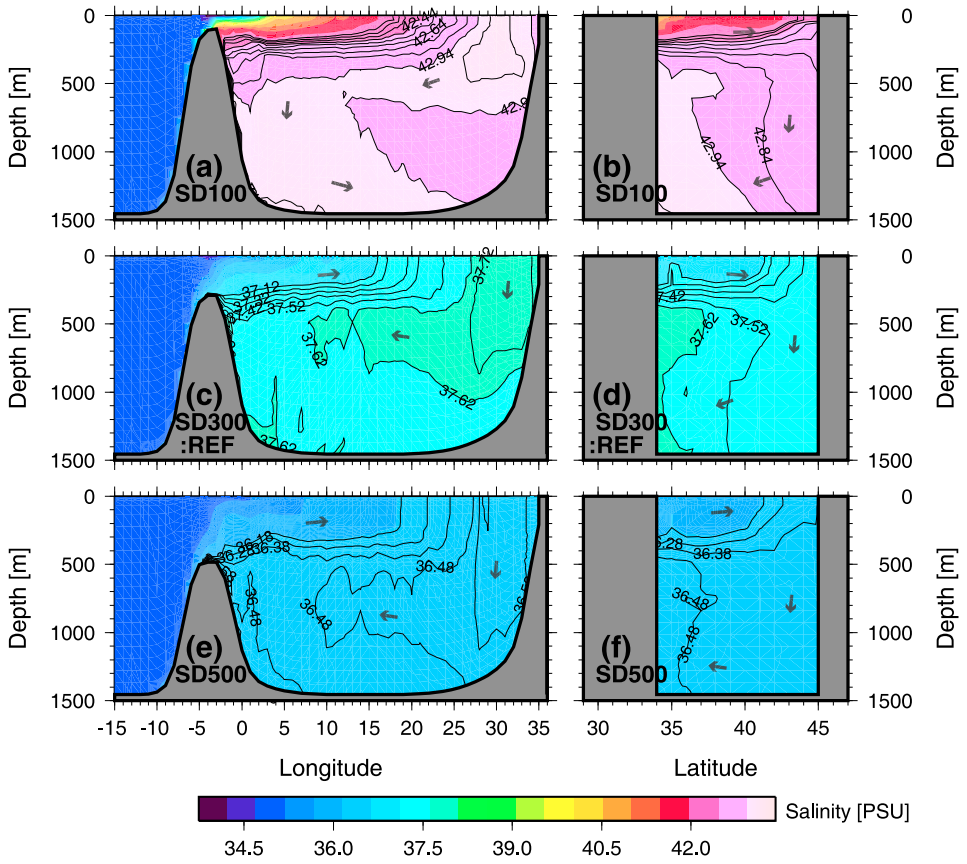

Figure 4. (a, c, and e) Zonal cross sections at 37°N (ZZ′ in Figure 1a). (b, d, and f) Meridional cross sections at 15°E (MM′ in Figure 1a) of the salinity fields averaged over the last 11 years of integration (years 990–1000) for the different experiments SD100 (Figures 4a and 4b), SD300:REF (Figures 4c and 4d), and SD500 (Figures 4e and 4f). Contour interval 0.1 psu, and arrows indicate the sense of transport.

of > 4.5 Sv in the basin center at ~300 m depth. We can compute the formation rate of the intermediate water from the zonal stream function (following *Dijkstra* [2008], *Ezer and Mellor* [1997], and *Rahmstorf and England* [1997]), by considering the volume of the downwelling water east of 25°E. We find that the model predicts a formation rate of ~2.5 Sv (Figure 7c). The closed streamlines on the right side of the gateway indicate a recirculation of ~1 Sv of the intermediate waters into the basin as part of the AW at the surface.

[22] The model reproduces the sinking of the dense water in the northern part of the basin near 15°E to flow eastward and fill the lower layers of the basin, feeding the deep zonal cell. The deep cell has a maximum absolute value of around ~1.25 Sv near 28°E at 1000 m depth. As the deep-water formation takes place in the northern part of the basin, the dense water sinks and spreads southward in the bottom layers. This process can be easily observed in the meridional stream function (Figure 7d). The meridional stream function has been computed for the part of the basin between longitudes 3°W and 36°E and thus provides a view of the area north of latitude 38°N (further south the segment is not limited by the coastline and the stream function may be distorted by flow in and out of our selected segment). It is with respect to the "corner" north of 43°N that we will quantify the rate of deep-water formation. Figure 7d clearly shows the sinking of dense water near the northern boundary of the basin and its southward spreading in the deep layers. About 1.5 Sv of the 3.5 Sv of the meridional cell sinks to the bottom north of 43°N. We find that the average rate of intermediate and deep water transformation over the last 10 years of the simulation is about 4 Sv over the entire basin.

[23] Time series of maximum and minimum values of the zonal overturning stream function and of maximum value of the meridional stream function have been computed in the basin and are presented in Figures 3c and 3d. These maximum and minimum values can be considered as an index of the MTHC variability (strengthening and weakening). Using this index we can monitor the evolution of the MTHC during the simulation and compare to the observations. The overturning stream function decreases during more than 200 years to converge toward an equilibrium state. The maximum (minimum) of the zonal stream function is about 4.22 (−1.38) Sv and the maximum of the meridional stream function is ~3.64 Sv at the end of the simulation.

3.1.3. Model Validation

[24] To assess the validity of the model predictions for the MTHC, it is important to weigh our model results against observations keeping in mind the coarse resolution and the

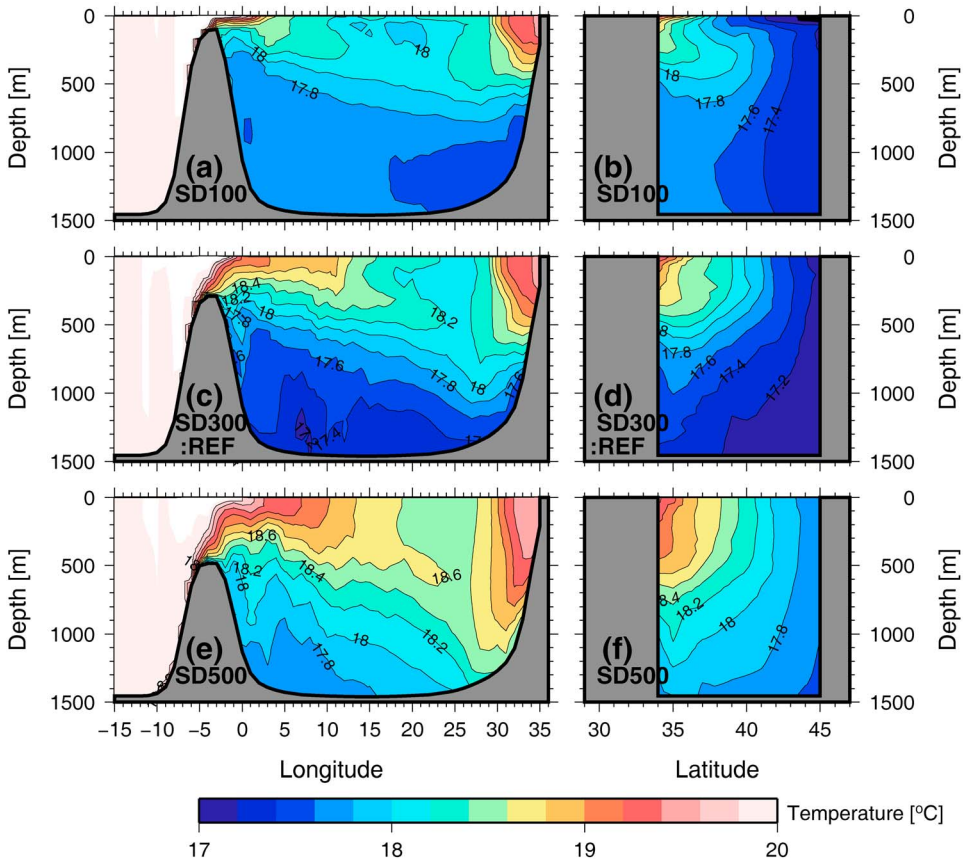

Figure 5. (a, c, and e) Zonal cross sections at 37°N (ZZ′ in Figure 1a). (b, d, and f) Meridional cross sections at 15°E (MM′ in Figure 1a) of the temperature fields averaged over the last 11 years of integration (years 990–1000) for the different experiments SD100 (Figures 5a and 5b), SD300:REF (Figures 5c and 5d), and SD500 (Figures 5e and 5f); contour interval 0.2°C.

idealized setup. It is of a crucial importance, given our objectives, to capture qualitative correct Mediterranean Sea circulation patterns and to obtain model transports of the correct order of magnitude. The model predicts an inflow of ~1.9 Sv (Table 1) which is almost a factor of two larger than the widely accepted estimate for the present day (1.1 Sv [*Bryden et al.*, 1994; *Tsimplis and Bryden*, 2000]). Still, the modeled value is quite acceptable comparing to observations at the high end of the range [i.e., *Bethoux*, 1980; *Pickard and Emery*, 1990] and to the value of 1.32 Sv reproduced by other simulations with POM [*Zavatarielli and Mellor*, 1995].

[25] The idealized basin geometry leads to a larger volume than the real Mediterranean Sea. This, combined with the modeled inflow, gives a residence time (basin volume divided by the inflow rate) of ~74 years (Table 2). This value is in good agreement with the present-day timescale of the Mediterranean overturning circulation of about 70 years [*Pickard and Emery*, 1990]. Also, the model depicts the flow system through the gateway in good agreement with both observations and other modeling studies. For example, the sinking and the northward flow of the Mediterranean outflow water are similar to the results of *Baringer and Price* [1997] and *Jungclaus and Mellor* [2000]; the eastward flow of the Atlantic water along the African coast as described by *Millot* [1999]; and the northward recirculation in the easternmost part of the basin [*Alhammoud et al.*, 2005, and references within]. Indeed, the vertical structure of the flow across the sill has the same shape as in the results of *Jungclaus and Mellor* [2000, Figure 11]. The interface depth and slope are in good agreement with estimates reported in previous studies [*Hopkins*, 1999; *Sannino et al.*, 2002; *Speich et al.*, 1996; *Tsimplis and Bryden*, 2000; *Vargas et al.*, 2006].

[26] In Appendix A we analyze the behavior of the model gateway in the light of analytical theory for flow through sea straits. Such theory starts from an assumption about the dynamics of strait flow. Two main concepts are hydraulic control and rotational control, applicable to straits that are, respectively, narrow and wide (the boundary between these being set by the Rossby radius of deformation). For each of the two dynamic regimes, theory allows one to derive a mathematical expression that relates (1) strait geometry, (2) strait transport, and (3) the salinity difference between ocean and basin. We apply these expressions by setting strait geometry to the model values and then entering the modeled salinities of basin and ocean to calculate the corresponding transport. By comparing this value to the transport found with

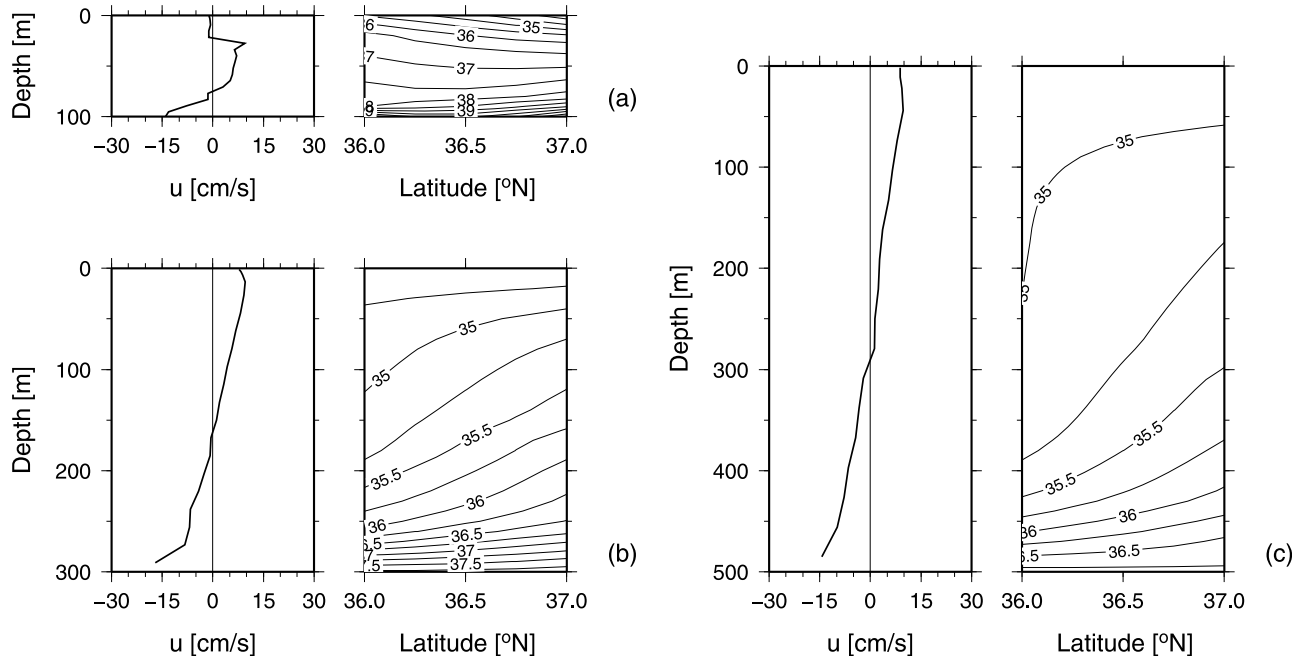

Figure 6. Along-strait flow velocity and across-strait salinity for three different experiments: (a) SD100, (b) SD300:REF, and (c) SD500. The east-west velocity is monitored right over the sill at longitude 3°W and in the middle of the strait (i.e., latitude 36.5°N). Eastward flow is positive. The meridional salinity section is also drawn at 3°W and shows isohalines interpolated between the two latitudes at which salinity is computed. The velocity profile would fall exactly halfway in this section. The contour interval for salinity is 0.5 psu in Figure 6a and 0.25 psu in Figures 6b and 6c.

the ocean circulation model we are able to judge to which extent the model strait complies with either hydraulic or rotational control. As shown in some detail in Appendix A it is found that the model gateway is most likely subject to rotational control, albeit it is in imperfect fashion because of the limited horizontal resolution. This proves to be true not only for a sill depth of 300 m but for a wide range of depths. In Appendix A we also show that the model provides us with combinations of strait transport, basin-to-ocean salinity difference and sill depth that are similar in value to the theoretical predictions for the case of hydraulic control in a strait much more narrow (13–16 km) than the actual model strait. This is an important finding as it implies that our model captures the type of gateway of interest to us. Even though the coarse-resolution model does not allow us to investigate in detail what happens in the strait, the model does seem to offer a fair representation of the effects of the strait on the water properties and circulation of the land-locked basin which are the focus of our analysis. However, the limitation of the current coarse resolution of the model grid motivates further experiments with higher resolution in the gateway region in the future.

[27] The vertical structure of the salinity and temperature (Figures 4c, 4d, 5c, and 5d) reveals that the simulated MTHC patterns satisfactory resemble those described in the literature [*Pinardi and Masetti*, 2000; *Somot*, 2005; *Wüst*, 1961; *Zavatarielli and Mellor*, 1995]. Despite the difference in the water mass characteristics (simulation of the water masses is not the aim of our study) the process of dense-water formation seems to be well pictured by the model, in agreement with observations [*MEDOC Group*, 1970; *Robinson et al.*, 1992]. Indeed, the location of the intermediate and deep water formation is accurately reproduced as well, respectively at the eastern and central northern parts of the basin. The formation rate of the intermediate water of ~2.5 Sv is slightly higher than the estimated rate found in literature which ranges between 0.6 Sv and 2.2 Sv [*Castellari et al.*, 2000; *Lascaratos et al.*, 1993; *Myers and Haines*, 2000; *Somot*, 2005; *Tziperman and Speers*, 1994; *Zavatarielli and Mellor*, 1995]. The total rate of intermediate and deep water formation over the whole Mediterranean basin is in good agreement with estimates of 6.4 Sv [*Castellari et al.*, 2000], 5.2 Sv [*Somot*, 2005] and 4 Sv [*Tziperman and Speers*, 1994]. From sensitivity experiments without SST relaxation (not shown), we find that the deep-water formation seems to be mainly controlled by the heat flux forcing, while the situation is completely different for the intermediate water formation which is mainly controlled by the salt flux, which is in agreement with *Somot et al.* [2006].

[28] The patterns of the zonal and meridional stream functions are in good agreement with those reproduced by previous modeling studies with higher resolution grid [*Castellari et al.*, 2000; *Lascaratos et al.*, 1993; *Myers and Haines*, 2000; *Somot*, 2005; *Tziperman and Speers*, 1994; *Zavatarielli and Mellor*, 1995]. The strength of the zonal and meridional stream function is overestimated with respect to the observations due to the idealized bottom geometry and the coarse resolution in the model. The maximum of the zonal stream function is twice as large as that found in other

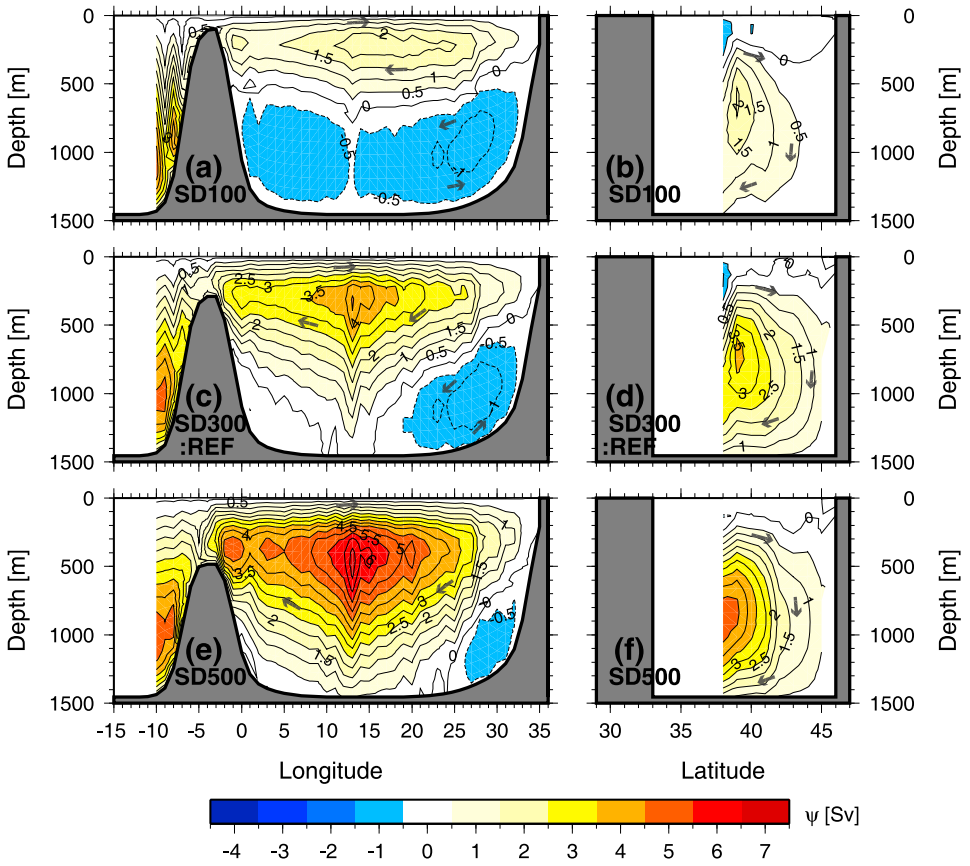

Figure 7. (a, c, and e) Zonal overturning stream function and (b, d, and f) meridional overturning stream function for the different experiments SD100 (Figures 7a and 7b), SD300:REF (Figures 7c and 7d), and SD500 (Figures 7e and 7f). Contour interval is 0.5 Sv, and arrows indicate the sense of transport; positive values correspond to clockwise circulation.

modeling studies [*Meijer et al.*, 2004; *Myers and Haines*, 2002; *Somot et al.*, 2006], but the patterns exhibit a good similarity. This strong zonal overturning maybe explains the low salinity of the intermediate layers by the overmixing with the adjacent waters or the short time exposure of AW to evaporation effects. The model results have revealed that the strong zonal overturning does not affect the overall patterns of the MTHC. For example, the vertical structure (two cells) and depths of the extrema of the zonal overturning are qualitatively in good agreement. It is worth noting that the ratio of the lower cell to the upper cell of the zonal overturning stream function for the present-day case are in agreement with those values inferred from previous modeling studies with higher resolution and more realistic setup (Table 1).

[29] Summarizing, the model reproduces qualitatively the flows through the ocean gateway and the processes of intermediate and deep-water formation in the basin, including their location. We thus find that the model captures some of the main aspects of the present-day MTHC. This validation of the model helps to elucidate the performance and the limitation of the model. The main purpose of our setup is not to study the regional details of the Mediterranean circulation, but to examine the large-scale changes of the overturning

Table 1. Volume Transport Through Gateway Into Basin, Stream Function Extrema, and Ratios of Stream Function Extrema as Reported in Literature and Found in This Study[a]

	Inflow (Sv)	Max Ψ_Z (Sv)	Min Ψ_Z (Sv)	Max Ψ_m (Sv)	$\lvert$Min $\Psi_Z\rvert$/Max Ψ_Z	Max Ψ_m/Max Ψ_Z	Max Ψ_m/$\lvert$Min $\Psi_Z\rvert$
Stratford et al. [2000]	0.70	0.75	−0.15	x	0.20	x	x
Myers and Haines [2002]	1.59	1.45	−0.50	x	0.34	x	x
Meijer et al. [2004]	0.80	1.25	−0.25	x	0.20	x	x
Somot et al. [2006]	1.17	1.50	−0.50	0.80	0.33	0.53	1.60
This study	1.92	4.22	−1.38	3.64	0.33	0.86	2.46

[a]Volume transport through the gateway into the basin is inflow. ψ_z and ψ_m are zonal and meridional stream functions, respectively.

Table 2. Dynamic and Hydrological Characteristics Averaged Over the Last 100 Years of Integration for All Experiments

Sill Depth (m)	Inflow (Sv)	Max Ψ_Z (Sv)	Min Ψ_Z (Sv)	Max Ψ_m (Sv)	S (psu)	T (°C)	Residence Time (year)	$\lvert$Min $\Psi_Z\rvert$/Max Ψ_Z	Max Ψ_m/Max Ψ_Z	Max Ψ_m/$\lvert$Min $\Psi_Z\rvert$
50	0.62	2.34	−1.26	2.20	46.10	17.73	230.39	0.54	0.94	1.75
100	0.69	2.40	−1.23	2.04	42.80	17.79	206.55	0.51	0.85	1.66
200	1.27	3.33	−1.31	2.70	38.93	17.72	111.71	0.39	0.81	2.06
300	1.92	4.22	−1.38	3.46	37.52	17.80	73.97	0.33	0.86	2.64
400	2.56	5.14	−1.08	4.32	36.85	18.12	55.57	0.21	0.84	4.00
500	3.21	6.25	−0.84	4.88	36.42	18.32	44.24	0.13	0.78	5.81
700	4.79	8.16	−0.35	5.78	35.81	18.74	29.76	0.04	0.71	16.51
900	4.75	9.33	−0.15	6.03	35.60	18.97	30.05	0.02	0.65	40.20

circulation in response to changes in the sill depth. For this it appears we may be confident in our model setup.

3.2. Role of Sill Depth

[30] Next, several sensitivity experiments are performed in order to investigate the effect of variation in sill depth. Here we present details only of experiments with sill depth 500 m and 100 m, referred as SD500 and SD100 respectively, which we compare to SD300:REF. From the temporal evolution of the kinetic energy measure (Figure 3a), SD500 is more energetic than SD100 and reaches the equilibrium state faster (~100 year for SD500 and ~600 year for SD100). The volume transport through the strait monotonically increases with sill depth (Table 2). The basin-averaged salinity at the end of the simulation for SD500 (~36.4 psu) is lower than in SD300:REF (~37.5 psu), while the SD100 exhibits higher salinity (~42.8 psu) (see also Figure 3b). The basin-averaged temperature at the end of the simulation from the SD500 (~18.3°C) is higher than SD300:REF values (~17.8°C), whereas the SD100 displays lower values (~17.7°C). The time series of the zonal and meridional stream function in the basin (Figure 3c) show that the zonal overturning of SD500 is quickly established and that the overturning circulation reaches the equilibrium state after ~100 years. On the contrary, the zonal overturning of SD100 decays gradually during the first 500 years to stabilize after then.

[31] In SD500, the inflow-outflow through the gateway displays almost the same structure as in SD300:REF (Figure 6). On the contrary, the SD100 experiment produces a more complex velocity-depth profile and salinity distribution. Only the lowest 20 m are occupied by the outflow from the Mediterranean. Also, in the surface layer, flow speed is essentially zero (due to strong variation of the surface current). The vertical distribution of the water masses remains almost the same as in SD300:REF (Figures 4 and 5). Besides the shift in the salinity and temperature values mentioned above, the halocline and thermocline are deeper in SD500 (400 m) and shallower in SD100 (~100 m), compared to SD300:REF (200–300 m). Consequently, the intermediate water is pushed downward to > 1000 m depth in SD500 and is uplifted to about 300 m depth in SD100 in the eastern part of the basin. Given the changes in the salinity and the outflow patterns in SD500 and SD100, one may expect some changes in the MTHC compared to SD300:REF.

[32] The zonal overturning circulation from SD500 and SD100 exhibits two significant changes in the flow pattern (Figures 7a, 7c, and 7e). First, as the sill depth increases, we observe an intensification of the clockwise cell in the upper layers and a weakening and reduction in extent of the counterclockwise cell in the deep layers. The clockwise cell extends almost over all the basin depth in SD500, while the counterclockwise cell fills the bottom layers of the basin below 500 m in SD100. A second feature is that the location of the maximum of the upper zonal cell shifts to shallower depths as the sill depth decreases, while the location of the minimum of the deep zonal cell shifts to greater depths. SD500 shows a maximum value of the upper zonal cell of ~6.5 Sv in the center of the basin and deeper than 500 m, while SD100 exhibits only ~2 Sv at 170 m depth. The maximum absolute value of the counterclockwise deep cell in SD500 is ~0.5 Sv and the cell is restricted to the bottom of the eastern part of the basin, while it shows a large value of ~1.5 Sv at ~850 m depth in SD100. The maximum of the upper zonal cell intensifies by 2 Sv (~44%) when the sill depth increases from 300 m to 500 m (66%), and the absolute value of the deep zonal cell decreases by about 1 Sv (66%). In SD500 (Figure 7e), ~3.5 Sv of the 6.5 Sv overturning sinks in the eastern part of the basin (east of 25°E) indicating the formation rate of the intermediate water, which decreases to ~1.5 Sv in SD100. However, judging from the counterclockwise cell of the zonal overturning combined with the zonal salinity sections, the shallow sill seems to generate a downwelling circulation near the gateway. This process leads to the recirculation of the westward flow of the intermediate waters, which intensifies the deep counterclockwise cell of the zonal overturning.

[33] The meridional cell increases in strength as the sill depth increases (Figures 7b, 7d, and 7f). The maximum value is about 2 Sv near 39°N in SD100 and ~4.5 Sv, shifted southward to < 38°N, in SD500. The streamlines show clearly the sinking of the dense water that is newly formed in the northern part of the basin and which forms the clockwise overturning cell, advecting the deep waters southward. Figure 7 allows us to estimate the deep-water formation rates (between 43°N and the northern boundary) which increase from ~0.5 Sv in SD100 to 1.5 Sv for SD500. These formation rates indicate an intensification of the deep convection in the northern part of the basin as the sill depth increases. To put it in the other way around, the ventilation of the basin deep layers diminishes as the sill depth decreases. The impact of the changes in the overturning circulation on the deep waters properties is evidenced by the east-west difference of temperature and salinity in the basin (Figure 8). The salinity and temperature difference between the eastern and western parts

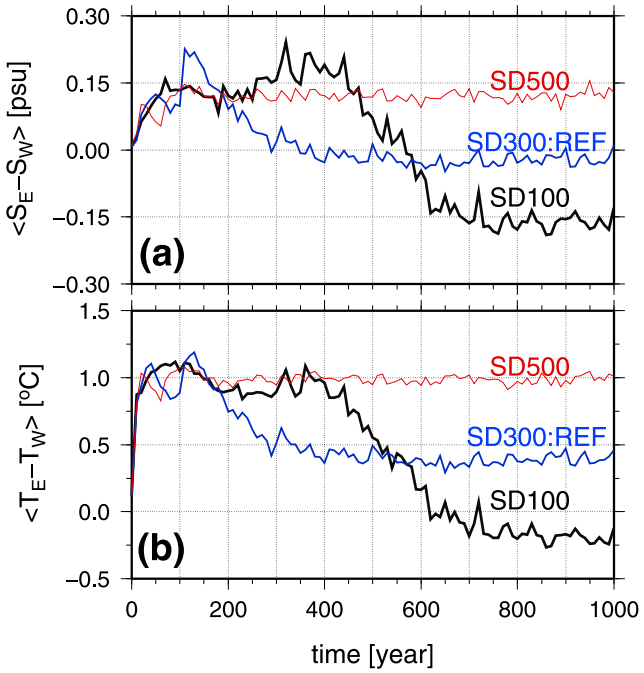

Figure 8. Time series from the different simulations SD300:REF (blue), SD100 (black), and SD500 (red) of spatial differences in salinity and temperature. (a) Decadally smoothed difference in salinity of the lower 500 m of boxes W and E in Figure 1a. (b) Same as Figure 8a but for temperature.

of the basin (S_E–S_W and T_E–T_W in Figure 1) is positive for SD500, while it decays gradually and tends to be negative for the SD100. In other words, with a shallow sill, the deep water in the west is more saline than in the east.

[34] The relationship between sill depth and overturning circulation is summarized in Table 2 and depicted in Figure 9. Experiments SD900, SD700, SD400, SD200 and SD050 are used in this section to refine the sensitivity of the thermohaline circulation to sill depth changes. First of all, the flow through the strait varies linearly with the sill depth (Table 2). The behavior of the overturning as a function of sill depth in Figure 9 can be divided in two parts, separated by the sill depth of 300 m (present-day value). The meridional cell (diamonds) and the upper zonal cell (circles) show almost similar behavior and a monotonic intensification as the sill depth increases while the intensity of the deep zonal cell (triangles) decreases. The meridional cell and the upper zonal cell exhibit a nonlinear intensification for sills shallower than 300 m and nearly linear intensification for sills deeper than 300 m. The strength of the deep zonal cell seems to be almost constant for shallow sills and becomes more sensitive to sill depth changes for deep sills. The sensitivity (i.e., slope) of the meridional cell (diamonds) to sill depth changes is weaker than the sensitivity of the upper zonal cell (circles). It is worth noting that the measure for the intensity of overturning does not take into account the occupied area (see Figure 7).

[35] The ratio of the strength of the meridional cell and the upper zonal cell displays a nearly constant value of 0.8 ± 0.15 (Table 2). In contrast, the strength ratio of the upper and deep zonal cells is constant for shallow sills, while it shows an exponential increase for deep sills. In other words, deep sills are combined with a stronger overturning and weaker recirculation in the bottom layers. Analysis of the scaling of the thermohaline circulation is beyond the scope of this work and will be addressed in a separate paper.

4. Discussion

[36] Despite the coarse horizontal resolution, the idealized basin geometry and the idealized forcing, the model demonstrates ability to reproduce most of the Mediterranean water masses reasonably well and replicates the main features of the Mediterranean thermohaline circulation. In particular, two key processes which control the MTHC, the flow through the strait and the formation of dense waters, are well matched qualitatively. Thus, we believe our simulations provide important insights into the effects of paleogeography on the thermohaline circulation. Our model has an advantage over analytical and box models in that it allows investigation of the 3-D structure of the circulation and spreading of water masses. In other words, the model not only allows us to see variations in the intensity of the THC, but also in the shape of the overturning cells and their 3-D extent within the basin. At the same time our model has the advantage over 3-D high-resolution numerical models that it entails a low computational cost.

4.1. Role of Sill Depth

[37] The model results illustrate that the antiestuarine circulation system is sustained through the experiments for all

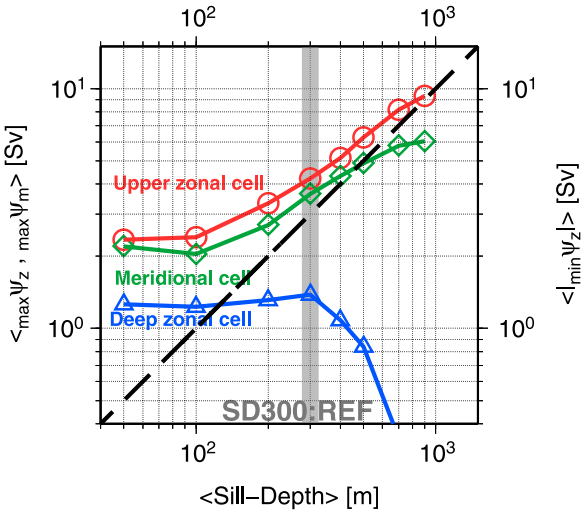

Figure 9. Strength of the Mediterranean thermohaline circulation as a function of sill depth as computed from values averaged over the last 100 years of integration (years 901–1000). Circle, maximum of zonal overturning; diamond, maximum of meridional overturning; and triangle, absolute value of minimum of zonal overturning (right vertical axis). The black dashed line indicates a slope equal to unity; the vertical shaded strip corresponds to the sill depth in SD300:REF (present-day value).

sill depths. As the only difference between the experiments is the depth of the ocean gateway, the modeled changes of the MTHC as described in the previous sections, must be related to what happens at the gateway.

[38] In experiment SD500, the deep connection of the Mediterranean Sea to the open ocean allows a stronger outflow and a quick flushing of the intermediate water from the Mediterranean basin compared to the SD300:REF. This implies, given the constraint of volume conservation, a strong inflow which produces a thicker layer of Atlantic water and a deeper thermocline in the basin. This strong inflow-outflow system explains the freshening and warming of the water column and the short residence time in the basin (Figure 3 and Table 2). In contrast, in SD100, the shallow sill hinders the outflow of the Mediterranean waters. When less water flows out, there is less need for a compensating inflow and the intensity of the inflow-outflow system is reduced. In its turn, a reduction in exchange leads to a rise of Mediterranean salinity (Figure 3), a shoaling of the thermocline (Figure 4a), and an increase of the residence time (Table 2).

[39] The deepening of the thermocline in SD500 favors deep convection in the easternmost part of the basin, i.e., in the region characterized by intermediate-water formation when sill depth is less. The "intermediate water" almost sinks to the bottom layers (Figures 4 and 5), overturning is very strong and the deep layers are well ventilated. This was also suggested by *Dijkstra* [2007] in the context of the characterization of the meridional overturning circulation in the Atlantic Ocean. Consequently, the characteristics of intermediate and deep water are very similar and the water column structure seems to consist of two water masses only, the AW and the intermediate/deep waters (Figures 4 and 5). Deepening of the upper zonal cell in SD500 may be said to suppress or replace the development of a separate deep counterclockwise cell.

[40] With a shallow sill (experiment SD100) the reduced intensity and depth extent of the upper zonal cell lead to a high stratification of the water column. Deep-water formation (Figure 7b) is reduced and the deeper parts of the basin are less well ventilated than in the case of greater sill depth. Probably because the upper cell extends less deep, the remaining deep-water formation drives a deep cell of greater extent in the eastern half of the basin (there is "more blue" east of 13°E in Figure 7a than there is in Figure 7b or Figure 7c). Deep water just east of the sill is (in SD100) no longer drawn up into the return flow to the Atlantic. Instead, we observe the deep cell to extend westward. Counterclockwise circulation in this western deep region may in part be driven by momentum imparted to the deeper layers by the westward flow above it. More importantly, it appears that the shallow sill forces part of the westward flowing intermediate water to return in a downwelling movement just east of the gateway. The salinity sections (Figure 4a) and the salinity difference between the eastern and western parts of the basin (Figure 8a) show the presence of relatively saline water at depth in the west which evidences this downward flow of the intermediate waters. Recently, on the basis of theoretical studies, *Iovino et al.* [2008] introduced the concept of the "blocking effect" regarding the role of sill depth on dense-water formation. Following these authors we refer to the downward flow just east of the sill also as a consequence of the blocking effect. While *Iovino et al.* [2008] focus on the impact of sill depth on convection, in particular, on the heat exchange driven by a boundary current, we focus on the overturning circulation. Our results show that a shallow sill, even though leading to a reduction in deep-water formation, does not cause the deep water to stagnate in the kinematic sense.

[41] Three different circulation modes of the MTHC can be identified and are shown schematically in Figure 10: (1) a shallow sill depth "SS" mode combined with a strong blocking effect leading to weak clockwise overturning (upper) cell and a strong and stretched counterclockwise (lower) one (Figures 7a and 10a); (2) a deep sill depth "DS" mode combined with weak blocking effect which implies a strong clockwise overturning (upper) cell and a reduced (almost shutdown) counterclockwise (lower) one (Figures 7c and 10c); (3) a moderate sill depth "MS" mode (present-day case) combined with a moderate blocking effect driving the coexistence of both clockwise and counterclockwise overturning cells (Figures 7b and 10b).

[42] A more detailed, quantitative, description of the various cells as a function of sill depth was presented in the form of Figure 9. In the interpretation of Figure 9 we may consider: (1) the upper (clockwise) cell of the zonal overturning (Figure 9, circles) as an indicator of the downward transport of intermediate water in the eastern part of the basin; (2) the deep (counterclockwise) cell of the zonal overturning (Figure 9, triangles) as an indicator of the upward transport (upwelling) of deep water in the eastern part of the basin; and (3) the (clockwise) cell of the meridional overturning (Figure 9, diamonds) as an indicator of the downward transport of deep waters in the northern part of the basin. For sills deeper than 400 m, the quasi-linear intensification of the upper zonal cell coincides with the increase in AW inflow (Table 2) suggesting that intermediate-water formation (being part of the upper cell) is directly related to the inflow through the strait. In contrast, the deep zonal cell displays nonlinear weakening (Figure 9, triangles) which suggests to us that the deep-water formation (essential to the deep cell) is partly controlled by the inflow through the gateway but also partly by the internal MTHC (upper cell).

4.2. Relating Model Results to the Sedimentary Record

[43] Our finding that reduced sill depth results in elevated basin salinity and increased residence time, both of which may be expected to have left their imprint in the geological record, is consistent with the predictions of simple budget considerations. The classical "Knudsen relations" express exactly this: the salinity difference between open ocean and restricted basin increases when the exchange between them is less [e.g., *Pond and Pickard*, 1983]. *Bryden and Stommel* [1984] complemented the equations for water and salt conservation with the notion of hydraulic control at the strait which allowed the authors to derive a relationship between basin salinity and sill depth. In this pioneering work a reduction in sill depth (in the form of a sea level lowering) was shown to result in a salinity increase of the basin (see also Appendix A). The Neogene sedimentary record of the Mediterranean provides dramatic evidence for raised salinity in the form of the evaporite deposits of the Messinian salinity

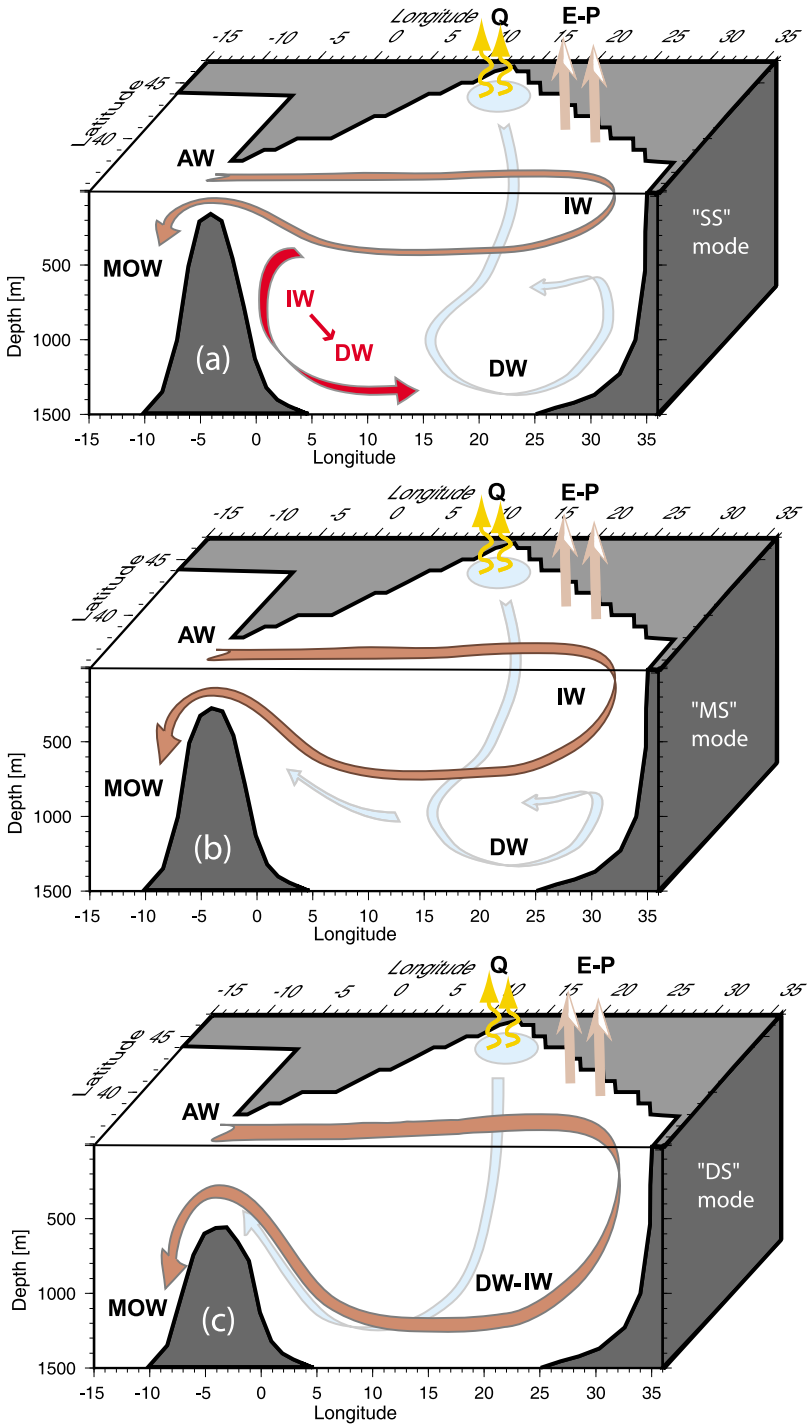

Figure 10. Schematic diagram of three circulation modes of antiestuarine thermohaline circulation in the Mediterranean Sea depending on sill depth. (a) Shallow sills "SS" mode, (b) moderate sills "MS" mode, and (c) deep sills "DS" mode. Dark brown indicates the upper cell of the zonal overturning in the basin. The light blue indicates the meridional overturning cell connected to the deep cell of the zonal overturning. The darkest red indicates the recirculation of intermediate waters into deep layers and its mixing with deep waters. Vertical zigzag arrows indicate the heat flux (Q), vertical straight arrows indicate the evaporation minus precipitation (E−P), and the circle indicates the zone of deep-water formation.

crisis (for a recent overview, see *CIESM* [2008] and *Hsü et al.* [1973]). The formation of these evaporites was most likely associated with extreme reduction of strait transport (see model analyses by *Blanc* [2006], *Meijer* [2006] and *Rohling et al.* [2008]).

[44] Paleoceanographic observations more pertinent to our model analysis are those related to the pre-Messinian record. In an early overview paper, *Vergnaud-Grazzini* [1985] already inferred that stable isotope data of benthic and planktonic foraminifera from the Mediterranean evidence an increase in residence time during the middle Miocene. The author tentatively linked these changes to an increasingly restricted connection to the Atlantic Ocean. More recently, *Kouwenhoven and van der Zwaan* [2006] and *Kouwenhoven et al.* [2006] (see also work by, e.g., *van der Zwaan et al.* [1999], *Kouwenhoven et al.* [1999], and *Seidenkrantz et al.* [2000]) presented geochemical proxies (element analysis: Mn/Al ratio; oxygen and carbon isotopes) and evaluation of faunal composition of benthic foraminifera for several late Miocene Mediterranean sections. The authors infer a trend of increasing salinity, increasing age and decreasing oxygen content of the deeper waters of the Mediterranean basin which started in the early Messinian at 7.2 Ma, that is, about 1.2 million years prior to the onset of evaporites deposition and thus to the Messinian salinity crisis (adopting ages of *Krijgsman et al.* [1999a]). *Kouwenhoven et al.* [2006] focus on the assemblage composition of calcareous nannofossils and foraminifera (planktonic and benthic) of a late Miocene section on Cyprus and find further evidence for decreasing oxygen content and increasing salinity of the deeper waters, changes that are consistent with the regional Mediterranean evolution. By the early Messinian the connection between the Mediterranean and the Atlantic Ocean had most likely been reduced to a single gateway through northwestern Africa, the so-called Rifian corridor [*Benson et al.*, 1991], the northern "Betic corridor" having closed earlier [*Garcés et al.*, 2001; *Soria et al.*, 1999]. Tectonostratigraphic studies in the Rifian corridor point to the occurrence of uplift during the early Messinian [*Krijgsman et al.*, 1999b; *van Assen et al.*, 2006] which provides geological evidence in support of a causal relationship between water properties and sill depth. Our model results are consistent with the suggested relationship and may thus be considered to provide additional, mechanism, physics-based, support for a dominant role of sill depth. In terms of our experiments the paleoceanographical data would seem to reflect a change from a situation similar to that at present (SD300) to that involving a more shallow sill (e.g., SD100). *Kouwenhoven and van der Zwaan* [2006] explicitly make the case that their data are consistent with the presence of two superimposed cells. This, according to the model results, rules out the presence of a deep sill in which the circulation is comprised of one cell only (e.g., SD500). It would be very interesting indeed to investigate whether the geological record for times prior to 7.2 Ma holds evidence for this "DS mode."

[45] Interestingly, our model results allow us to add detail to one important aspect of the intuitively expected consequences of gateway restriction as they are, for example, expressed in the above mentioned observational studies: shoaling of the sill does not seem to necessarily lead to a true stagnation of the deeper waters. As shown in Figure 7a and, schematically, in Figure 10a, the model predicts a shallow sill to be associated with a marked deep cell. This, however, does not imply good ventilation of the deep layers: the deep cell is largely fed by water that is blocked from flowing out to the ocean, not by deeply convected, oxygenated, surface water. This effect has also been observed in the response of the MTHC to the precession minimum conditions in a very high resolution (5x5 km) modeling experiment (B. Alhammoud et al., unpublished results, 2007). We suggest it would be very interesting to explore whether this behavior can be confirmed from observations. Another result of our work that would seem to form a hypothesis worth testing is the quasi-constant ratio between the strength of the meridional cell and that of the upper zonal cell ($\sim 0.8 \pm 0.15$; see 10th column in Table 2).

[46] Our model consists of a single land-locked basin communicating with the "outside ocean" but the results are most likely equally applicable to the sedimentary record of the western Mediterranean basin as they are to that of the eastern basin. In the latter case, however, the relevant sill depth would be that of the Strait of Sicily or its precursor. This point was recently made by *Köhler et al.* [2010] in their interpretation of the Tortonian record of Mt. Gibliscemi on Sicily which, at the time the sediments were deposited, occupied a position in the eastern basin. *Meijer et al.* [2004] performed a first model experiment of the role of the depth of the connection between the western and eastern subbasin and observed the same response as reported in the present study.

[47] Our model analysis may form the basis for an investigation of Mediterranean circulation during the Last Glacial Maximum when global sea level lowering was responsible for the Gibraltar sill being situated at a depth about 120 m less than at present. To do this properly, however, we would also need to adjust the atmospheric forcing and Atlantic salinity [cf. *Bigg*, 1994; *Bozec et al.*, 2007; *Myers et al.*, 1998a].

[48] Although aimed specifically at the Eurafrican Mediterranean Sea, our model analysis, precisely because it considers an idealized basin shape and simple atmospheric forcing, should be applicable to other basins as well. Examples that are nearby in all respects would be the basins of the Oligocene-Miocene Paratethys realm but one might also think of the Atlantic basin in the early stages of its opening during the Mesozoic.

5. Conclusions

[49] Several sensitivity experiments of the Mediterranean thermohaline circulation were conducted using the Princeton Ocean Model with an idealized geometry and climatic forcing. Our simulated present-day circulation was compared to observations and previous numerical studies. Subsequently, we analyzed the impact of changes in sill depth. The results have been related to observations and hypotheses concerning the late Miocene circulation of the Mediterranean Sea. Our main conclusions are the following.

[50] 1. A much idealized, "minimal," model is still capable of capturing the main feature of the present-day MTHC and to reproduce the process of deep-water formation. This opens the way to model investigations of the basin-scale circulation

in the geological past under geographical and climatological conditions markedly different from those at present.

[51] 2. A shallow sill induces a blocking effect on the outflow of intermediate and deep waters. This provides a mechanism to explain the increase of salinity and poor ventilation of the Mediterranean Sea during periods of restricted connection to the open ocean.

[52] 3. Three different circulation modes have been identified depending on the sill depth: shallow sill "SS," moderate sill "MS," and deep sill "DS," coupled with strong, weak and almost zero blocking effects, respectively. The SS mode is characterized by a weak clockwise upper overturning cell and a strong and stretched counterclockwise deep one. The MS mode reflects the present-day thermohaline circulation patterns, while the DS mode is combined with strong clockwise overturning (upper) cell and a reduced (almost shutdown) counterclockwise (deep) one.

[53] 4. Model results are consistent with the interpretation of paleoceanographical data for the early Messinian and thus offer support for the notion that, at least at certain times, change in sill depth played a decisive role in the evolution of Mediterranean water properties and circulation.

[54] 5. A strong deep zonal cell of the overturning circulation does not strictly imply strong ventilation. In contrast, a weakening of deep overturning cell leads definitely to ventilation weakening. In other words, a stagnation certainly induces oxygen depletion, while the opposite is not true; the oxygen depletion does not always indicate a circulation stagnation.

Appendix A

[55] Here we compare the behavior of the strait in our numerical model to the predictions of analytical theory developed for straits. Whereas the numerical model solves, in the strait just as it does elsewhere, the full equation of motion, the essence of analytical strait theory is that a clever choice is made of the terms that are expected to dominate in a certain configuration (see, notably, *Whitehead* [1998]). The theory then consists of solving the idealized equation of motion in combination with conservation laws of water and salt. Here we will consider perhaps the most commonly cited two cases, that of hydraulically controlled strait flow and that of so-called rotational control.

[56] Both theories, at least in their basic form as applied here, relate to steady flow (i.e., no temporal variation in velocity or density), neglect internal as well as bottom friction, and assume an absence of mixing between the opposed flows. Whereas the first condition is readily met by considering annual means of the model-derived fields, the other aspects do not hold true for the numerical results. For example, Figure 6 clearly shows the mixing of salinity between inflow and outflow. Also, our model includes a nonzero parameterization of horizontal mixing and involves a nonzero bottom friction. Still, it is also because of these differences that it is of interest to try and quantify to which extent the model strait behaves consistent with analytical theory.

[57] Fundamental to the concept of hydraulic control is the notion that, for narrow straits where Coriolis force can also be neglected, the equation of motion, subject to all of the above mentioned simplifications, reduces to a statement of balance between the horizontal pressure gradient and the inertia term (i.e., the term expressing advection of momentum). The horizontal pressure gradient arises from the density difference between inflow and outflow in conjunction with along-strait variation in the depth of their mutual interface [see also *Officer*, 1976]. A second principle underlying hydraulic control is that flow velocity attains the maximum possible value under the given density difference. It is only under this condition that the problem has a single solution. *Bryden and Kinder* [1991], following upon the seminal paper by *Bryden and Stommel* [1984], review a series of expressions for hydraulically controlled strait transport. We take the expression devised originally by *Farmer and Armi* [1986] for a strait of rectangular cross section where control is imposed by the presence of a sill, rather than by a horizontal contraction. This would seem to best match our model setup where the strait is wide. The expression reads

$$Q_A = Q_M = 0.208\sqrt{g'H}HW$$

with Q_A is inflow transport from the Atlantic, Q_M is outflow transport, H is sill depth, W is strait width, and g' is reduced gravity,

$$g' = g\frac{\rho_M - \rho_A}{\rho_M}$$

In this g is the acceleration of gravity, ρ_A is density of the Atlantic water, and ρ_M is density of Mediterranean water. The expression for transport is derived under the assumption that inflow and outflow are approximately the same. In other words, it ignores the presence of the small net inflow that is to compensate for net evaporation over the Mediterranean. In evaluating the ratio of densities we follow *Bryden and Stommel* [1984] in their assumption that salinity is the main variable responsible for density variation and we use a (their) linearized equation of state,

$$\rho_A = \rho_{ref} + \beta\,(S_A - S_{ref})$$

and likewise for ρ_M. Here $\rho_{ref} = 1027$ kg m^{-3}, $S_{ref} = 36.5$ psu, and $\beta = 0.77$ kg m^{-3} psu^{-1} from *Bryden and Stommel* [1984]. As to the salinities S_A and S_M we took, respectively, the salinity in the Atlantic "sponge" of 35 psu and the basin-averaged salinity found in the numerical experiment for each sill depth (Table 2). The transport values thus found for hydraulic control by the sill in a 222 km wide strait prove an order of magnitude larger than the modeled transports. For example, with a sill depth of 300 m, hydraulic control predicts a value of 3.3 Sv which we should compare to the 1.9 Sv found in the numerical model. It clearly follows that the strait in the ocean circulation model is not subject to hydraulic control. Viewed in more detail it proves that the ratio between the prediction of hydraulic control theory and the model-derived value is more or less the same for all sill depths. Since hydraulically controlled transport scales linearly with strait width (see equation above) this leads to the suggestion that, in terms of strait transports, our numerical model is behaving consistent with hydraulic control in a strait much more narrow than 222 km. This suggestion is confirmed graphically

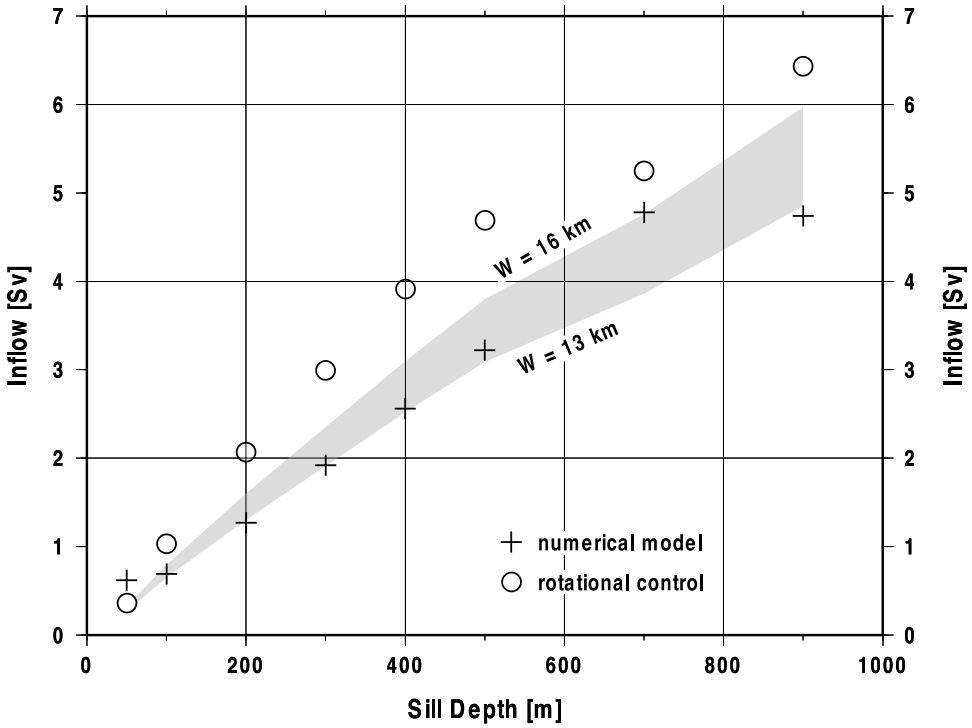

Figure A1. Comparison between modeled inflow transport as a function of sill depth (crosses) and estimates based on strait theory. The latter estimates are calculated using the modeled basin average salinity to determine the density of the outflow water. The shaded band relates to the transport predicted for the case of hydraulic control of strait flow. The upper and lower limits of this band correspond to an assumed strait width of 16 km and 13 km, respectively. The circles give, for each sill depth considered, the inflow one would expect if strait flow was rotationally controlled. See text for discussion.

in Figure A1: our model-derived estimates for inflow are consistent with hydraulic control when strait width lies in the limited range of 13–16 km.

[58] As an alternative to hydraulic control we considered the possibility of rotational control. In this case the basic assumption is that there exists geostrophic balance in the across-strait direction. In other words, it is assumed that there is a balance between (1) the across-strait pressure gradient due to the tilt of the density interface between inflow and outflow and (2) the Coriolis force. Rotational control is expected to become important when strait width exceeds the Rossby radius. The presence of tilted salinity contours in Figure 6 seems to point to a role of rotation in our model results. This is not surprising given the large width.

[59] An expression for transport in a strait of rectangular cross section, governed by rotational control, was derived by *Whitehead* [1998] subject to many of the same assumptions underlying the hydraulic control theory outlined above: steady, frictionless, nonmixing flow and taking inflow and outflow transport to be essentially the same. In addition, the rotational control theory assumes negligible deflection of the sea surface and conservation of potential vorticity. The expression reads

$$Q_A = Q_M = 0.156\frac{g'H^2}{f}$$

in which g' and H are reduced gravity and sill depth as before and f is the Coriolis parameter. Calculating the ratio of densities in the same way as for hydraulic control this expression gives us the transports plotted in Figure A1 together with the modeled values. For sill depths between 100 and 500 m the rotationally controlled value is consistently a factor 1.5–1.6 larger than the modeled value. For the other sill depths relative differences are smaller.

[60] The finding that modeled combinations of strait transport and salinity difference between basin and ocean lie much closer to the values for rotational control than to those of hydraulic control suggests that, in the model, strait transport is rotationally controlled. The associated processes are not expected to be captured in any detail though, given the coarse resolution and limited numbers of nodes in the gateway. This limited resolution, but also differences between the representations by model and theory (spelled out in the above) and assumptions made in our application of the theory, are all potentially responsible for the mismatch between model result and theoretical prediction in Figure A1. However, the fact that Coriolis force plays a role in the model behavior has been ascertained by varying (for a sill depth of 300 m) the Coriolis parameter in the vicinity of the strait. In this case the model-derived transport was found to vary consistent with the predictions of the rotational control equation. In contrast, variation of the bottom friction (being another candidate for controlling strait flow in the model) was

found to affect the short-term variability of the transport but not its average value and does therefore not seem to be a dominant factor.

[61] To summarize, we have shown in here that, in terms of underlying mechanism, it appears the model gateway is dominated by rotational effects. In addition, the model yields combinations of strait transport, basin-to-ocean salinity contrast, and sill depth, that are, in value, comparable to the predictions of hydraulic control theory for strait widths much less than in the numerical model. This is an important result as it implies that we may be confident our model captures the type of gateway behavior of relevance to our problem. There are several factors that may explain why the wide model gateway behaves similar to a more narrow hydraulically controlled strait. Assuming that rotational effects dominate gateway behavior in our model, the reason for this is first of all the simple fact that rotational control is an effective mechanism. For the same sill depth and density difference between basin and ocean, rotational control corresponds to transports comparable in size to the hydraulically controlled value in a much narrower strait. In other words, our calculations merely illustrate a property of the two control mechanisms. Moreover, using the same model-derived variation of basin-to-ocean salinity difference as a function of sill depth, both rotational control (thought to characterize our model results) and hydraulic control predict a quasi-linear relationship between transport and sill depth (Figure A1). Note that it is only at first glance that the previous statement appears to contradict the equations given above. Even though the equations for hydraulic and rotational control feature different dependence between transport Q and sill depth H, the density difference, represented by reduced gravity g′, also varies with sill depth.

[62] **Acknowledgments.** This work has been done in the context of the Utrecht Center of Geosciences. Computational resources were provided by the Netherlands Research Center for Integrated Solid Earth Science (ISES 3.2.5 High End Scientific Computation Resources). We would like to express our gratitude to Tanja Kouwenhoven, Wout Krijgsman, Pasha Karami, and, in particular, Rinus Wortel for invaluable discussions and stimulating suggestions. We thank Mike Rogerson and an anonymous reviewer for their constructive criticisms on the previous version of the manuscript. Figures have been prepared using GMT [*Wessel and Smith*, 1998].

References

Alhammoud, B., K. Béranger, L. Mortier, M. Crépon, and I. Dekeyser (2005), Surface circulation of the Levantine Basin: Comparison of model results with observations, *Prog. Oceanogr.*, *66*(2–4), 299–320, doi:10.1016/j.pocean.2004.07.015.

Baringer, M. O., and J. F. Price (1997), Mixing and spreading of the Mediterranean outflow, *J. Phys. Oceanogr.*, *27*, 1654–1676, doi:10.1175/1520-0485(1997)027<1654:MASOTM>2.0.CO;2.

Beckers, J. M., et al. (2002), Model intercomparison in the Mediterranean: MEDMEX simulation of the seasonal cycle, *J. Mar. Syst.*, *33–34*, 215–251, doi:10.1016/S0924-7963(02)00060-X.

Benson, R. H., K. Rakic-El Bied, and G. Bonaduce (1991), An important current reversal (influx) in the Rifian Corridor (Morocco) at the Tortonian-Messinian boundary: The end of Tethys Ocean, *Paleoceanography*, *6*(1), 165–192, doi:10.1029/90PA00756.

Bethoux, J. P. (1980), Mean water fluxes across sections in the Mediterranean Sea, evaluated on the basis of water and salt budgets and of observed salinities, *Oceanol. Acta*, *3*(1), 79–88.

Bigg, G. R. (1994), An ocean general circulation model view of the glacial Mediterranean thermohaline circulation, *Paleoceanography*, *9*(5), 705–722, doi:10.1029/94PA01183.

Blanc, P.-L. (2006), Improved modelling of the Messinian salinity crisis and conceptual implications, *Palaeogeogr. Palaeoclimatol. Palaeoecol.*, *238*, 349–372, doi:10.1016/j.palaeo.2006.03.033.

Blumberg, A. F., and G. L. Mellor (1987), A description of a three-dimensional coastal ocean circulation model, in *Three-Dimensional Coastal Ocean Models, Coastal Estuarine Sci. Ser.*, vol. 4, edited by N. S. Heaps, pp. 1–16, AGU, Washington, D. C.

Bozec, A., M. Kageyama, G. Ramstein, and M. Crépon (2007), Impact of a Last Glacial Maximum sea-level drop on the circulation of the Mediterranean Sea, *Geophys. Res. Abstr.*, *9*, 03935, sref:1607-7962/gra/EGU2007-A-03935.

Bryden, H. L., and T. H. Kinder (1991), Steady two-layer exchange through the Strait of Gibraltar, *Deep Sea Res., Part A*, *38*, S445–S463.

Bryden, H. L., and H. M. Stommel (1984), Limiting processes that determine basic features of the circulation in the Mediterranean Sea, *Oceanol. Acta*, *7*(3), 289–296.

Bryden, H. L., J. Candela, and T. H. Kinder (1994), Exchange through the Strait of Gibraltar, *Prog. Oceanogr.*, *33*(3), 201–248, doi:10.1016/0079-6611(94)90028-0.

Candela, J. (2001), The Mediterranean water and global circulation, in *Observing and Modelling the Global Ocean*, edited by J. Siedler et al., pp. 419–429, Academic, San Diego, Calif.

Castellari, S., N. Pinardi, and K. Leaman (2000), Simulation of water mass formation processes in the Mediterranean Sea: Influence of the time frequency of the atmospheric forcing, *J. Geophys. Res.*, *105*(C10), 24,157–24,181, doi:10.1029/2000JC900055.

CIESM (2008), The Messinian salinity crisis from mega-deposits to microbiology-A consensus report, in *CIESM Workshop Monographs, Rep.* 33, edited by F. Briand, pp. 1–168, Monaco.

Dijkstra, H. A. (2007), Characterization of the multiple equilibria regime in a global ocean model, *Tellus, Ser. A*, *59*(5), 695–705, doi:10.1111/j.1600-0870.2007.00267.x.

Dijkstra, H. A. (2008), Scaling of the Atlantic meridional overturning circulation in a global ocean model, *Tellus, Ser. A*, *60*(4), 749–760.

Drakopoulos, P., and A. Lascaratos (1999), Modelling the Mediterranean Sea: Climatological forcing, *J. Mar. Syst.*, *20*, 157–173, doi:10.1016/S0924-7963(98)00080-3.

Duggen, S., K. Hoernie, P. Van den Bogaard, L. Rüpke, and J. P. Morgan (2003), Deep roots of the Messinian salinity crisis, *Nature*, *422*, 602–606, doi:10.1038/nature01553.

Ezer, T., and G. L. Mellor (1994), Diagnostic and prognostic calculations of the North Atlantic circulation and sea level using a sigma coordinate ocean model, *J. Geophys. Res.*, *99*(C7), 14,159–14,171, doi:10.1029/94JC00859.

Ezer, T., and G. L. Mellor (1997), Simulations of the Atlantic Ocean with a free surface sigma coordinate ocean model, *J. Geophys. Res.*, *102*(C7), 15,647–15,657, doi:10.1029/97JC00984.

Farmer, D. M., and L. Armi (1986), Maximal two-layer exchange over a sill and through the combination of a sill and contraction with barotropic flow, *J. Fluid Mech.*, *164*, 53–76, doi:10.1017/S002211208600246X.

Garcés, M., W. Krijgsman, and J. Agustí (2001), Chronostratigraphic framework and evolution of the Fortuna Basin (eastern Betics) since the late Miocene, *Basin Res.*, *13*, 199–216, doi:10.1046/j.1365-2117.2001.00144.x.

Gill, A. E. (1982), *Atmosphere-Ocean Dynamics*, 662 pp., Academic, Orlando, Fla.

Haines, K., and P. Wu (1995), A modelling study of the thermohaline circulation of the Mediterranean Sea: Water formation and dispersal, *Oceanol. Acta*, *18*(4), 401–417.

Haug, G. H., and R. Tiedemann (1998), Effect of the formation of the Isthmus of Panama on Atlantic Ocean thermohaline circulation, *Nature*, *393*, 673–676, doi:10.1038/31447.

Hermann, A. J., P. B. Rhines, and E. R. Johnson (1989), Nonlinear Rossby adjustment in a channel: Beyond Kelvin waves, *J. Fluid Mech.*, *205*, 469–502, doi:10.1017/S0022112089002119.

Hopkins, T. S. (1999), The thermohaline forcing of the Gibraltar exchange, *J. Mar. Syst.*, *20*, 1–31, doi:10.1016/S0924-7963(98)00068-2.

Horton, C., M. Clifford, J. Schmitz, and L. H. Kantha (1997), A real-time oceanographic nowcast/forecast system for the Mediterranean Sea, *J. Geophys. Res.*, *102*(C11), 25,123–25,156, doi:10.1029/97JC00533.

Hsü, K. J. (1983), *The Mediterranean Was a Desert: A Voyage of Discovery*, 197 pp., Princeton Univ. Press, Princeton, N. J.

Hsü, K. J., W. B. F. Ryan, and M. R. Cita (1973), Late Miocene desiccation of the Mediterranean, *Nature*, *242*, 240–244, doi:10.1038/242240a0.

Iovino, D., F. Straneo, and M. A. Spall (2008), On the effect of a sill on dense water formation in a marginal sea, *J. Mar. Res.*, *66*(3), 325–345, doi:10.1357/002224008786176016.

Jolivet, L., R. Augier, C. Robin, J.-P. Suc, and J. M. Rauchy (2006), Lithosphere-scale geodynamic context of the Messinian salinity crisis, *Sediment. Geol.*, *188–189*, 9–33, doi:10.1016/j.sedgeo.2006.02.004.

Jungclaus, J. H., and G. L. Mellor (2000), A three-dimensional model study of the Mediterranean outflow, *J. Mar. Syst.*, *24*, 41–66, doi:10.1016/S0924-7963(99)00078-0.

Köhler, C. M., D. Heslop, W. Krijgsman, and M. J. Dekkers (2010), Late Miocene paleoenvironmental changes in North Africa and the Mediterranean recorded by geochemical proxies (Monte Gibliscemi section, Sicily), *Palaeogeogr. Palaeoclimatol. Palaeoecol.*, *285*, 66–73.

Korres, G., A. Lascaratos, E. Hatziapostolou, and P. Katsafados (2002), Towards an ocean forecasting system for the Aegean Sea, *Global Atmos. Ocean Syst.*, *8*(2–3), 191–218, doi:10.1080/1023673029000003534.

Kouwenhoven, T. J., and G. J. van der Zwaan (2006), A reconstruction of late Miocene Mediterranean circulation patterns using benthic foraminifera, *Palaeogeogr. Palaeoclimatol. Palaeoecol.*, *238*, 373–385, doi:10.1016/j.palaeo.2006.03.035.

Kouwenhoven, T. J., M.-S. Seidenkrantz, and G. J. van der Zwaan (1999), Deep-water changes: The near-synchronous disappearance of a group of benthic foraminifera from the late Miocene Mediterranean, *Palaeogeogr. Palaeoclimatol. Palaeoecol.*, *152*, 259–281.

Kouwenhoven, T. J., C. Morigi, A. Negri, S. Giunta, W. Krijgsman, and J.-M. Rouchy (2006), Paleoenvironmental evolution of the eastern Mediterranean during the Messinian: Constraints from integrated microfossil data of the Pissouri basin (Cyprus), *Mar. Micropaleontol.*, *60*, 17–44, doi:10.1016/j.marmicro.2006.02.005.

Krijgsman, W., F. J. Hilgen, I. Raffi, F. J. Sierro, and D. S. Wilson (1999a), Chronology, causes and progression of the Messinian salinity crisis, *Nature*, *400*, 652–655, doi:10.1038/23231.

Krijgsman, W., C. G. Langereis, W. J. Zachariasse, M. Boccaletti, G. Moratti, R. Gelati, S. Iaccarino, G. Papani, and G. Villa (1999b), Late Neogene evolution of the Taza-Guercif Basin (Riffan Corridor, Morocco) and implications for the Messinian salinity crisis, *Mar. Geol.*, *153*, 147–160, doi:10.1016/S0025-3227(98)00084-X.

Lascaratos, A., and K. Nittis (1998), A high-resolution three-dimensional numerical study of intermediate water formation in the Levantine Sea, *J. Geophys. Res.*, *103*(C9), 18,497–18,511, doi:10.1029/98JC01196.

Lascaratos, A., R. G. Williams, and E. Tragou (1993), A mixed-layer study of the formation of Levantine Intermediate Water, *J. Geophys. Res.*, *98*(C8), 14,739–14,749, doi:10.1029/93JC00912.

Li, L., A. Bozec, S. Somot, K. Béranger, P. Bouruet-Aubertot, F. Sevault, and M. Crépon (2006), Regional atmospheric, marine processes and climate modeling, in *Mediterranean Climate Variability*, edited by P. Lionello et al., pp. 373–397, Elsevier, Amsterdam.

Lionello, P., P. Malanotte-Rizzoli, R. Boscolo, and J. Luterbacher (2006), The Mediterranean climate: An overview of the main characteristics and issues, in *Mediterranean Climate Variability*, edited by P. Lionello et al., pp. 1–26, Elsevier, Amsterdam.

Marshall, J., and F. Schott (1999), Open-ocean convection: Observations, theory, and models, *Rev. Geophys.*, *37*, 1–64, doi:10.1029/98RG02739.

MEDOC Group (1970), Observation of formation of deep water in the Mediterranean Sea, 1969, *Nature*, *227*, 1037–1040, doi:10.1038/2271037a0.

Meijer, P. T. (2006), A box model of the blocked-outflow scenario for the Messinian salinity crisis, *Earth Planet. Sci. Lett.*, *248*, 471–479, doi:10.1016/j.epsl.2006.06.013.

Meijer, P. T., and H. A. Dijkstra (2009), The response of Mediterranean thermohaline circulation to climate change: A minimal model, *Clim. Past*, *5*, 713–720.

Meijer, P. T., and W. Krijgsman (2005), A quantitative analysis of the desiccation and re-filling of the Mediterranean during the Messinian salinity crisis, *Earth Planet. Sci. Lett.*, *240*, 510–520, doi:10.1016/j.epsl.2005.09.029.

Meijer, P. T., R. Slingerland, and M. J. R. Wortel (2004), Tectonic control on past circulation of the Mediterranean Sea: A model study of the late Miocene, *Paleoceanography*, *19*, PA1026, doi:10.1029/2003PA000956.

Mellor, G. L. (1991), An equation of state for numerical models of oceans and estuaries, *J. Atmos. Oceanic Technol.*, *8*, 609–611, doi:10.1175/1520-0426(1991)008<0609:AEOSFN>2.0.CO;2.

Mellor, G. L., and A. F. Blumberg (1985), Modeling vertical and horizontal diffusivities with the sigma coordinate system, *Mon. Weather Rev.*, *113*, 1379–1383, doi:10.1175/1520-0493(1985)113<1379:MVAHDW>2.0.CO;2.

Mellor, G. L., and T. Yamada (1982), Development of a turbulence closure model for geophysical fluid problems, *Rev. Geophys.*, *20*, 851–875, doi:10.1029/RG020i004p00851.

Mellor, G. L., T. Ezer, and L.-Y. Oey (1994), The pressure gradient conundrum of sigma coordinate ocean models, *J. Atmos. Oceanic Technol.*, *11*(4), 1126–1134, doi:10.1175/1520-0426(1994)011<1126:TPGCOS>2.0.CO;2.

Meulenkamp, J. E., and W. Sissingh (2003), Tertiary palaeogeography and tectonostratigraphic evolution of the northern and southern Peri-Tethys platforms and the intermediate domains of the African-Eurasian convergent plate boundary zone, *Palaeogeogr. Palaeoclimatol. Palaeoecol.*, *196*, 209–228, doi:10.1016/S0031-0182(03)00319-5.

Mikolajewicz, U., E. Maier-Reimer, T. J. Crowley, and K.-Y. Kim (1993), Effect of Drake and Panamanian gateways on the circulation of an ocean model, *Paleoceanography*, *8*(4), 409–426, doi:10.1029/93PA00893.

Millot, C. (1987), Circulation in the western Mediterranean Sea, *Oceanol. Acta*, *10*(2), 143–149.

Millot, C. (1999), Circulation in the western Mediterranean Sea, *J. Mar. Syst.*, *20*, 423–442, doi:10.1016/S0924-7963(98)00078-5.

Murdock, T. Q., A. J. Weaver, and A. F. Fanning (1997), Paleoclimatic response of the closing of the Isthmus of Panama in a coupled ocean-atmosphere model, *Geophys. Res. Lett.*, *24*(3), 253–256, doi:10.1029/96GL03950.

Myers, P. G., and K. Haines (2000), Seasonal and interannual variability in a model of the Mediterranean under derived flux forcing, *J. Phys. Oceanogr.*, *30*, 1069–1082, doi:10.1175/1520-0485(2000)030<1069:SAIVIA>2.0.CO;2.

Myers, P. G., and K. Haines (2002), Stability of the Mediterranean's thermohaline circulation under modified surface evaporative fluxes, *J. Geophys. Res.*, *107*(C3), 3021, doi:10.1029/2000JC000550.

Myers, P. G., K. Haines, and E. Rohling (1998a), Modeling the paleocirculation of the Mediterranean: The Last Glacial Maximum and the Holocene with emphasis on the formation of sapropel S_1, *Paleoceanography*, *13*(6), 586–606, doi:10.1029/98PA02736.

Myers, P. G., K. Haines, and S. Josey (1998b), On the importance of the choice of wind stress forcing to the modeling of the Mediterranean Sea circulation, *J. Geophys. Res.*, *103*(C8), 15,729–15,749, doi:10.1029/98JC00784.

Officer, C. B. (Ed.) (1976), *Physical Oceanography of Estuaries (and Associated Coastal Waters)*, 465 pp., John Wiley, New York.

Ovchinnikov, I. M. (1966), Circulation in the surface and intermediate layers of the Mediterranean, *Oceanology, Engl. Transl.*, *6*, 48–57.

Pickard, G. L., and W. J. Emery (Eds.) (1990), *Descriptive Physical Oceanography: An Introduction*, 5th ed., 320 pp., Pergamon, Oxford, U. K.

Pinardi, N., and E. Masetti (2000), Variability of the large scale general circulation of the Mediterranean Sea from observations and modelling: A review, *Palaeogeogr. Palaeoclimatol. Palaeoecol.*, *158*, 153–173, doi:10.1016/S0031-0182(00)00048-1.

Pond, S., and G. L. Pickard (1983), *Introductory Dynamical Oceanography*, 2nd ed., 329 pp., Pergamon, Oxford, U. K.

Popov, S. V., F. Rögl, A. Y. Rozanov, F. F. Steiniger, I. G. Scherba, and M. Kovac (2004), *Lithological-Paleogeographic Maps of Paratethys: 10 Maps Late Eocene to Pliocene, Cour. Forschungsinst. Senckenberg*, 250, 46 pp.

Rahmstorf, S., and M. H. England (1997), Influence of Southern Hemisphere winds on North Atlantic Deep Water flow, *J. Phys. Oceanogr.*, *27*, 2040–2054, doi:10.1175/1520-0485(1997)027<2040:IOSHWO>2.0.CO;2.

Robinson, A. R., et al. (1992), General circulation of the eastern Mediterranean, *Earth Sci. Rev.*, *32*, 285–309, doi:10.1016/0012-8252(92)90002-B.

Roether, W., B. B. Manca, B. Klein, D. Bregant, D. Georgopoulos, V. Beitzel, V. Kovacevic, and A. Luchetta (1996), Recent changes in eastern Mediterranean Deep Waters, *Science*, *271*, 333–335, doi:10.1126/science.271.5247.333.

Rogerson, M., E. J. Rohling, and P. P. E. Weaver (2006), Promotion of meridional overturning by Mediterranean-derived salt during the last deglaciation, *Paleoceanography*, *21*, PA4101, doi:10.1029/2006PA001306.

Rögl, F. (1998), Palaeogeographic considerations for Mediterranean and Paratethys seaways (Oligocene to Miocene), *Ann. Naturhist. Mus. Wien, Ser. A*, *99*, 279–310.

Rohling, E. J., and F. J. Hilgen (1991), The eastern Mediterranean climate at times of sapropel formation: A review, *Geol. Mijnbouw*, *70*, 253–264.

Rohling, E. J., R. Schiebel, and M. Siddall (2008), Controls on Messinian lower evaporite cycles in the Mediterranean, *Earth Planet. Sci. Lett.*, *275*, 165–171, doi:10.1016/j.epsl.2008.08.022.

Rossignol-Strick, M. (1985), Mediterranean Quaternary sapropels, an immediate response

of the African monsoon to variation of insolation, *Palaeogeogr. Palaeoclimatol. Palaeoecol.*, *49*, 237–263, doi:10.1016/0031-0182(85)90056-2.

Sannino, G., A. Bargagli, and V. Artale (2002), Numerical modeling of the mean exchange through the Strait of Gibraltar, *J. Geophys. Res.*, *107*(C8), 3094, doi:10.1029/2001JC000929.

Seidenkrantz, M.-S., T. J. Kouwenhoven, F. J. Jorissen, N. J. Shackleton, and G. J. van der Zwaan (2000), Benthic foraminifera as indicators of changing Mediterranean-Atlantic water exchange in the late Miocene, *Mar. Geol.*, *163*, 387–407.

Sierro, F. J., J. A. Flores, G. Francés, A. Vazquez, R. Utrilla, I. Zamarreño, H. Erlenkeuser, and M. A. Barcena (2003), Orbitally controlled oscillations in planktic communities and cyclic changes in western Mediterranean hydrography during the Messinian, *Palaeogeogr. Palaeoclimatol. Palaeoecol.*, *190*, 289–316, doi:10.1016/S0031-0182(02)00611-9.

Somot, S. (2005), *Modélisation climatique du bassin Méditerranéen: Variabilité et scénarios de changement climatique*, Ph.D. thesis, 239 pp., Univ. Paul Sabatier Toulouse III, Toulouse, France.

Somot, S., F. Sevault, and M. Déqué (2006), Transient climate change scenario simulation of the Mediterranean Sea for the twenty-first century using a high-resolution ocean circulation model, *Clim. Dyn.*, *27*(7–8), 851–879, doi:10.1007/s00382-006-0167-z.

Soria, J. M., J. Fernández, and C. Viseras (1999), Late Miocene stratigraphy and palaeogeographic evolution of the intramontane Guadix Basin (central Betic Cordillera, Spain): Implications for an Atlantic-Mediterranean connection, *Palaeogeogr. Palaeoclimatol. Palaeoecol.*, *151*, 255–266, doi:10.1016/S0031-0182(99)00019-X.

Speich, S., G. Madec, and M. Crépon (1996), A strait outflow circulation process study: The case of the Alboran Sea, *J. Phys. Oceanogr.*, *26*, 320–340, doi:10.1175/1520-0485(1996)026<0320:ASOCPS>2.0.CO;2.

Stratford, K., R. G. Williams, and P. G. Myers (2000), Impact of the circulation on sapropel formation in the eastern Mediterranean, *Global Biogeochem. Cycles*, *14*(2), 683–695.

Thorpe, R. B., and G. R. Bigg (2000), Modelling the sensitivity of Mediterranean outflow to anthropogenically forced climate change, *Clim. Dyn.*, *16*(5), 355–368, doi:10.1007/s003820050333.

Tsimplis, M. N., and H. L. Bryden (2000), Estimation of the transports through the Strait of Gibraltar, *Deep Sea Res., Part I*, *47*, 2219–2242, doi:10.1016/S0967-0637(00)00024-8.

Tziperman, E., and K. Speers (1994), A study of water mass transformation in the Mediterranean Sea: Analysis of climatological data and a simple three-box model, *Dyn. Atmos. Oceans*, *21*, 53–82, doi:10.1016/0377-0265(94)90004-3.

van Assen, E., K. F. Kuiper, N. Barhoun, W. Krijgsman, and F. J. Sierro (2006), Messinian astrochronology of the Melilla Basin: Stepwise restriction of the Mediterranean-Atlantic connection through Morocco, *Palaeogeogr. Palaeoclimatol. Palaeoecol.*, *238*, 15–31, doi:10.1016/j.palaeo.2006.03.014.

van der Zwaan, G. J., I. A. P. Duijnstee, M. Den Dulk, S. R. Ernst, N. T. Jannink, and T. J. Kouwenhoven (1999), Benthic foraminifers: Proxies or problems? A review of paleoecological concepts, *Earth Sci. Rev.*, *46*, 213–236.

Vargas, J. M., J. García-Lafuente, J. Candela, and A. J. Sánchez (2006), Fortnightly and monthly variability of the exchange through the Strait of Gibraltar, *Prog. Oceanogr.*, *70*(2–4), 466–485, doi:10.1016/j.pocean. 2006.07.001.

Vergnaud-Grazzini, C. (1985), Mediterranean Late Cenozoic stable isotope record: Stratigraphic and Paleoclimatic implications, in *Geological Evolution of the Mediterranean Basin*, edited by D. J. Stanley and F. C. Wezel, pp. 413–451, Springer, New York.

von der Heydt, A., and H. A. Dijkstra (2006), Effect of ocean gateways on the global ocean circulation in the late Oligocene and early Miocene, *Paleoceanography*, *21*, PA1011, doi:10.1029/2005PA001149.

Wessel, P., and W. H. F. Smith (1998), New, improved version of generic mapping tools released, *Eos Trans. AGU*, *79*(47), 579, doi:10.1029/98EO00426.

Whitehead, J. A. (1998), Topographic control of oceanic flows in deep passages and straits, *Rev. Geophys.*, *36*, 423–440, doi:10.1029/98RG01014.

Winton, M., and E. S. Sarachik (1993), Thermohaline oscillations induced by strong steady salinity forcing of ocean general circulation models, *J. Phys. Oceanogr.*, *23*, 1389–1410, doi:10.1175/1520-0485(1993)023<1389:TOIBSS>2.0.CO;2.

Wüst, G. (1961), On the vertical circulation of the Mediterranean Sea, *J. Geophys. Res.*, *66*(10), 3261–3271, doi:10.1029/JZ066i010p03261.

Xoplaki, E., J. F. Gonzalez-Rouco, J. Luterbacher, and H. Wanner (2004), Wet season Mediterranean precipitation variability: Influence of large-scale dynamics and trends, *Clim. Dyn.*, *23*(1), 63–78, doi:10.1007/s00382-004-0422-0.

Zavatarielli, M., and G. L. Mellor (1995), A numerical study of the Mediterranean Sea circulation, *J. Phys. Oceanogr.*, *25*, 1384–1414, doi:10.1175/1520-0485(1995)025<1384:ANSOTM>2.0.CO;2.

B. Alhammoud, Laboratoire de Météorologie Dynamique, Ecole Polytechnique, F-91128 Palaiseau CEDEX, France. (bahjat.alhammoud@lmd.polytechnique.fr)

H. A. Dijkstra, UCG, IMAU, Department of Physics and Astronomy, Utrecht University, NL-3584 CC Utrecht, Netherlands.

P. T. Meijer, UCG, Department of Earth Sciences, Faculty of Geosciences, Utrecht University, NL-3584 CD Utrecht, Netherlands.